Carbonates and Evaporites (2020) 35:12
https://doi.org/10.1007/s13146-019-00536-w

ORIGINAL ARTICLE

Petrophysical and acoustic characteristics of Jurassic and Cretaceous rocks from Central Lebanon

Mohamed K. Salah[1] · Mohammad Alqudah[2] · Ali J. Monzer[1] · Christian David[3]

Accepted: 12 December 2019 / Published online: 3 January 2020

Abstract
We conducted several petrophysical and acoustic measurements on 49 core samples collected from the Jurassic and Cretaceous strata exposed at west central Lebanon to evaluate their petrophysical and elastic properties and study the effects of the depositional conditions, sediment composition, and subsequent diagenetic processes on the measured parameters. First, these rocks were petrographically studied to identify their facies, porosity, and the main diagenetic features. In addition, these rocks were investigated under the scanning electron microscope (SEM) and by the X-ray diffraction (XRD) analysis to identify their mineralogy. The petrophysical measurements were performed on the core samples where porosity, permeability, bulk, and grain densities were first determined, followed by measuring the seismic wave velocities under dry and water-saturation conditions. Both carbonates and siliciclastics are encountered in the studied formations. The SEM and XRD analyses revealed that the main constituting minerals are quartz, calcite and dolomite. The studied rocks have generally low to moderate porosity and very low permeability with averages of 0.05, and 0.31 mD, respectively. The bulk density is moderate to high and varies narrowly between 2.03 and 2.79 with an average of 2.64 g/cm^3, whereas the average grain density is 2.77 g/cm^3. The average primary and secondary wave velocities (V_p and V_s) are 4263, and 2323 m/s, respectively, with an average V_p/V_s of 1.83. Water-saturation has significantly impacted the elastic properties of the studied rocks. From the obtained measurements, we further calculated the elastic coefficients of the studied rocks and constructed several relationships between the measured properties to investigate their mutual interdependence and evaluate the effects of porosity, rock composition, depositional and diagenetic processes on the rock characteristics. We found that some samples, mainly carbonates, deviate significantly from the expected porosity-velocity and density-velocity trends. Originally present micro- and intercrystalline pores and characteristic diagenetic processes in these carbonate rocks, and possibly coring-induced microcracking in few samples, may account for the observed outliers.

Keywords Jurassic and Cretaceous rocks · Central Lebanon · Petrophysics · V_p and V_s · Elastic moduli

Introduction

Acoustic measurements are important for both characterizing reservoir rocks in hydrocarbon exploration/zonation and the geo-mechanical assessment of Earth's materials for engineering applications (Siegesmund and Dürrast 2014; Ersoy et al. 2016; Yu et al. 2016). For this reason, seismic wave velocities have long been discussed by many investigators (e.g., Hughes and Kelly 1952; Brandt 1955; Hicks and Berry 1956; Wyllie et al. 1958; Nur and Simmon 1969; Elliot and Wiley 1975; Gregory 1976; Minear 1982; Han et al. 1986; Vernik and Nur 1992a, b; El Sayed et al. 1998, 2015). Primary and secondary wave velocities (V_p and V_s) are mainly related to the elastic coefficients which are controlled by the mineral composition, density, porosity, fluid type, saturation, compaction, laminations, fracturing, clay content and pore geometry, and are thus fundamental parameters of Earth materials (Han et al. 1986; Han and Batzle 2004; Wang et al. 2009a; Gupta and Sharma 2012; Tandon and Gupta 2013; Yu et al. 2016). The values and depth variation of the seismic wave velocities and density are important for

✉ Mohamed K. Salah
ms264@aub.edu.lb

[1] Department of Geology, American University of Beirut, Riad El Solh, 1107 2020 Beirut, Lebanon

[2] Geology Department, Faculty of Science, Yarmouk University, Irbid 21163, Jordan

[3] Department of Geosciences and Environment, University of Cergy-Pontoise, 95031 Cergy-Pontoise, France

characterizing subsurface geological structures, geotectonics, faulting mechanisms, evaluating seismic hazards, and strong ground motions (Wang et al. 2009a).

Among the various factors affecting velocity, porosity has the dominant control (Erickson and Jarrard 1998). Higher porosity leads to lower bulk density, lower rock rigidity and incompressibility, and accordingly, lower V_p and V_s (Gregory 1976). According to Han et al. (1986), the clay content in siliciclastic rocks is the next most important factor influencing seismic velocity. Moreover, the mode of clay occurrence impacts also the seismic velocity where suspended clays in the pores of sandstone have a small effect on velocity compared to structure and laminated clays which result in a significant velocity reduction (Minear 1982). Therefore, both the shale fraction and porosity were often included in the empirical relationships between velocity and porosity in low-porosity ranges (Castagna et al. 1985; Han et al. 1986). Velocity increases logarithmically with depth and the associated increase in overburden pressure, while the corresponding increase in temperature decreases it (Brandt 1955).

Carbonate rocks are economically important Earth materials and host about 50–60% of the oil and gas reserves around the world (e.g., Burchette 2012). Carbonate reservoirs have heterogeneous pore systems and a variety of grain types which control their elastic properties as well as other reservoir parameters (Neto et al. 2014). Such complex pore type variations result in large differences of seismic velocity at a given porosity (Sun et al. 2006) and overall complicated velocity–porosity relationships (Sun et al. 2015). In these situations, the study of the relationships between the elastic properties and other petrophysical parameters is important to understand and improve practical rock physics models. These relationships are also significant for calibrating porosity estimation techniques from sonic logs and seismic stacking velocities (Erickson and Jarrard 1998).

Porosity in carbonate rocks may be primary, including intergranular or intercrystalline pores or secondary comprising oomoldic, moldic, and vuggy pores (Anselmetti and Eberli 1999). Secondary pores are usually rounded and enforce the stiffness of rocks compared to interparticle pores, thus inducing greater seismic velocities, whereas microporosity and fractures are normally flat and cause the rocks to be softer (Berryman 1995; Kumar and Han 2005; Wang et al. 2009b; Xu and Payne 2009; Zhan et al. 2012). Therefore, the pore geometry and complexity in carbonate rocks strongly affect their permeability and elastic properties (e.g., Berryman and Blair 1987; Mavko et al. 1998; Saleh and Castagna 2004; Kumar and Han 2005). Unlike siliciclastic or shaly sediments, pure carbonate rocks exhibit little direct correlation between seismic wave velocities and age or burial depth (Anselmetti and Eberli 1993). Rather, seismic velocities are controlled more by the combined effect of lithology and the diagenetic processes such as cementation, recrystallization, and dissolution. Accordingly, the observed velocities of carbonates exhibit wider ranges, which are induced mainly by the amount and type of porosity but not by mineralogy. Deviations from both the direct trends between velocity and density in one hand, and the inverse trends between velocity and porosity on the other hand, maybe as high as 2500 m/s in carbonate rocks (Anselmetti and Eberli 1993). These large differences are produced by the occurrence of different pore types which may originate at later diagenetic phases.

In Lebanon, carbonate rocks are widely distributed and represent a very important natural resource of engineering and construction materials. The major karst aquifers are hosted in carbonate rocks (Doummar et al. 2012). In addition, development projects such as construction of dams and tunnels, cutting and widening of roads deal essentially with these rocks. Therefore, the present study is concerned with the quantification of the various petrophysical and elastic properties of a suite of rocks from west-central Lebanon dominated by carbonates with few sandstone samples. We establish many empirical interrelationships between the various measured properties which are significant for predicting some parameters from others (Ojha and Sain 2014) and compare some of them with published relationships. We end finally with a discussion focusing on the effects of mineralogical composition and diagenetic processes on the petrophysical and elastic properties of the studied rocks.

Geologic setting and lithostratigraphy

Lebanon, located between latitudes 32° 34′ N, and 34° 41′ N and longitudes 35° 05′ E and 36° 34′ E, stretches at the eastern margin of the Mediterranean Sea. It is situated in the northwestern corner of the Arabian Plate; one of the minor tectonic plates in the northern and eastern hemispheres (Beydoun 1977). The Levant Fracture System (LFS) which extends from the Gulf of Aqaba northwards to the Taurus Mountains in southern Turkey is a series of strike-slip faults propagating northwards as a result of the Red Sea rifting starting at the Oligocene/Miocene (Beydoun 1999). The LFS is a sinistral fault system which begins in the south with the N–S Dead Sea Fault System, comprises the central NNE–SSW-oriented Yamouneh Fault and splays (Fig. 1), and ends in the north with the N–S Ghab Fault (e.g., Develle et al. 2011; Ghalayini et al. 2014). Of these, the central Lebanon section is the most complex as it branches and veers to the right resulting in a restraining bend which, in turn, resulted in the high topography of the Lebanese Mountains (Daëron et al. 2007). According to Walley (1997), Lebanon is structurally divided into three NNE–SSW aligned areas: a synclinorium known as the elevated upland basin of the Bekaa that is Neogene infilled and two anticlinoria: Mount Lebanon and the eastern high Anti-Lebanon Range

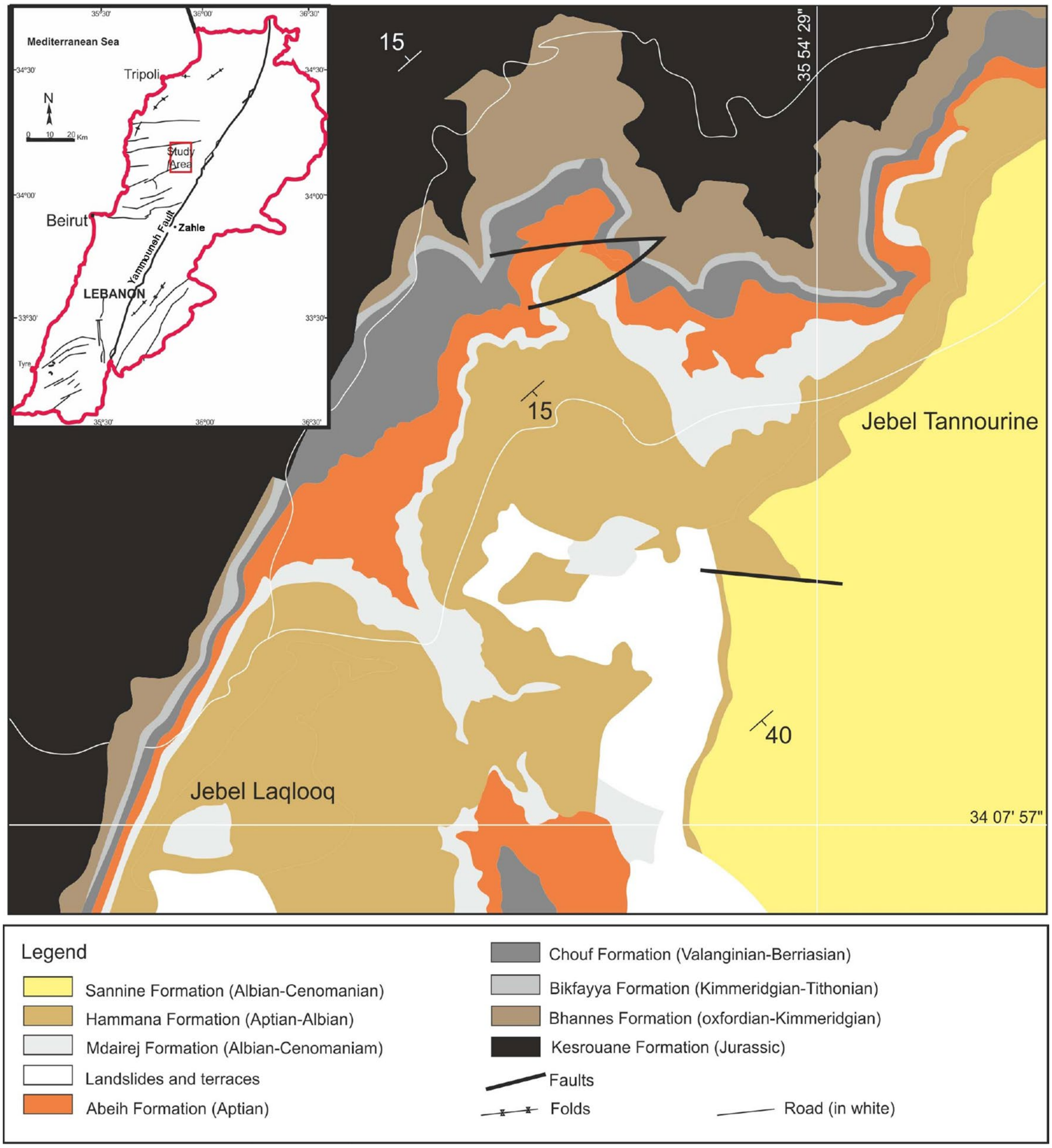

Fig. 1 Geological map of Lebanon (modified after Dubertret 1955). Inset to the upper left shows the geographic boundaries of Lebanon with a red rectangle showing the study area

which are Jurassic cored. The two anticlinoria border the Bekaa syncline from the west and east, respectively. These mountain ranges are major uplifts induced by a transpressive regime at the Lebanese segment of the LFS, with Late Cretaceous rocks forming the highest point of Mount Lebanon at 3088 m, and Middle Jurassic rocks forming the summit of Mount Hermon of the Anti-Lebanon range at 2814 m (e.g., Beydoun 1999; Gomez et al. 2006; Hawie et al. 2013). Mount Lebanon, to the west of the Bekaa valley, is a huge monocline dipping to the west with a semi-arid climate, while the Anti-Lebanon range has a more arid climate and a karstified terrain (Walley 1998). The NNE–SSW-oriented Yammouneh fault is a major fault in Lebanon, where it delineates the western border of the Bekaa depression and is believed to follow the western flank of the Dead Sea rift (Fig. 1). It was formed as a consequence of the northward movement of the Arabian plate and runs parallel to the eastern flank of Mount Lebanon. Other faults are also found in Lebanon but are of a smaller scale. The uplifting event induced by the transpressive regime led to the exposure of the Jurassic carbonate cores of the Lebanese Mountains

(Khair et al. 1997; Nader 2014); hence they were subjected to meteoric diagenesis and karstification (Nader et al. 2008).

Jurassic and Cretaceous strata in Lebanon, successively from older to younger, are represented by the following formations: Kesrouane (J_4), Bhannes (J_5), Bikfaya (J_6), Chouf (C_1), Abeih (C_{2a}), Mdairej (C_{2b}), Hammana (C_3), Sannine (C_4), Maameltein (C_5) and Chekka (C_6). The Jurassic rocks were deposited in a shallow marine carbonate platform environment (Hawie et al. 2014), while the Cretaceous facies include clastic deposits. In the present study, we sampled the Kesrouane Formation (Early to Late Jurassic) upward to the Abeih Formation, which is of Lower Cretaceous age (Fig. 2). A total of 29 samples were collected from the Kesrouane Formation (K1–K29), eight from Bikfaya (B1–B8), ten from the Chouf (TC1–TC10), and four from the Abeih Formation (TA1–TA4). The Kesrouane Formation (Walley 1998) is known as a bulk of heavily fractured and karstified carbonate rocks ranging in thickness from 1000 to ~ 1500 m,

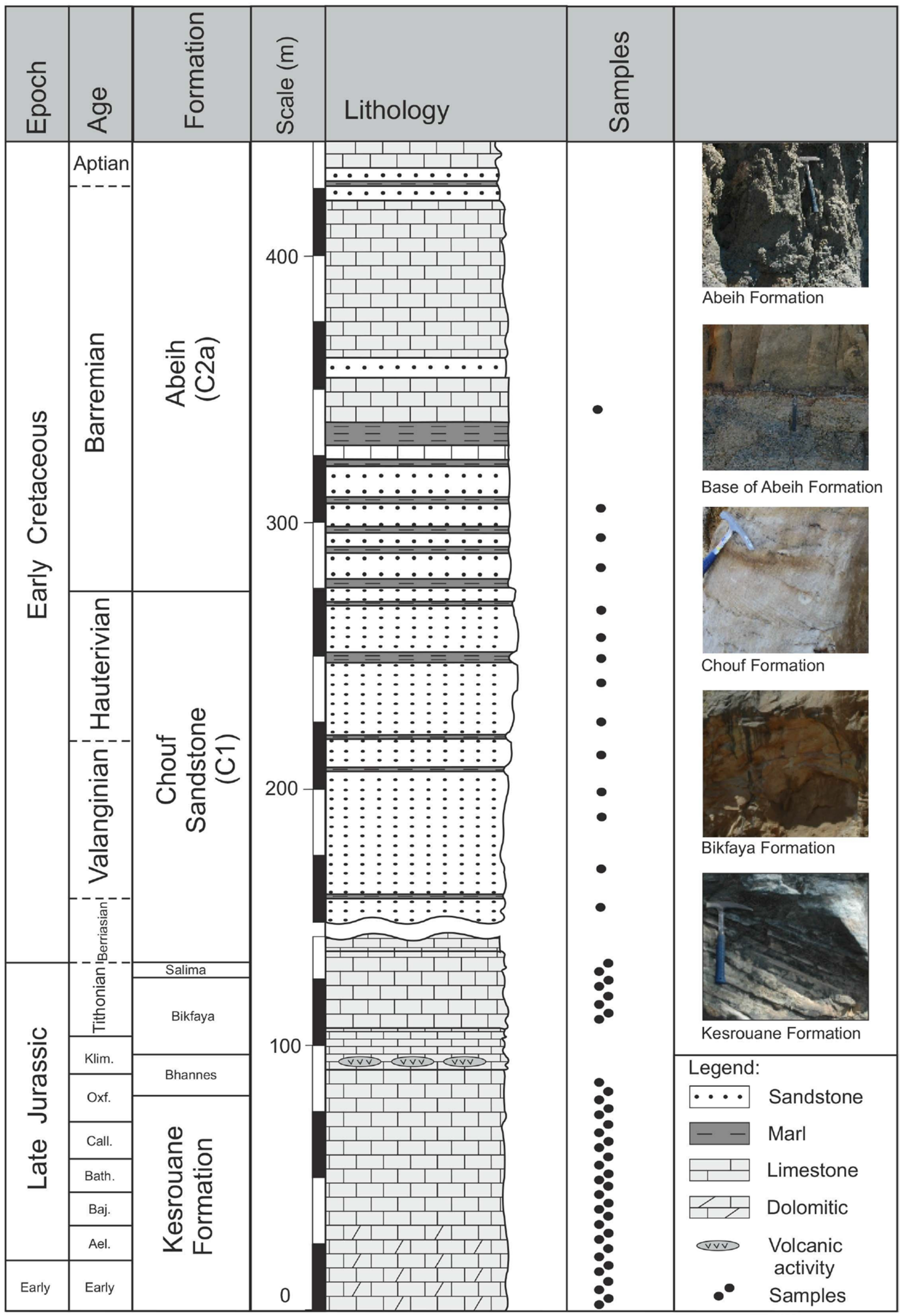

Fig. 2 Columnar section displaying the ages, names of the formations, dominant lithology, sample locations, and some field photographs for the studied rock units in west-central Lebanon (modified after Walley 1983)

with prevailing dolostone and micritic limestone (Dubertret 1955). Further petrologic and stratigraphic features of the rocks belonging to the Kesrouane Formation can be found elsewhere in other texts (e.g., Renouard 1955; Walley 1998; Nader and Swennen 2004).

The Kesrouane Formation is overlain by the Bhannes Formation, which has a thickness of 50–150 m and is composed of carbonate rocks, marls, basalts, and pyroclasts (Walley 1997). The basalts are related to Late Jurassic-Early Cretaceous volcanism which is observed only in northern Lebanon (Nader 2014) and occur as upward extensions in the overlying carbonate rocks emanating from open cracks related to the LFS enabling deep decompression melting and subsequent magma ascent (Adiyaman and Chorowicz 2002). The Bhannes Formation is separated from the overlying Bikfaya Formation by a nonconformity as an igneous body underlies a sedimentary stratum (Nader 2000) and forms an aquiclude above the underlying the Kesrouane Formation.

The Bikfaya Formation is Late Kimmiridgian to Early Tithonian in age (Dubertret 1975; Walley 1997). The thickness of this rock unit is variable but is probably around 60–80 m thick in the type area and is characterized by a prominent cliff-forming pale-brownish grey carbonate unit that often contains chert nodules, siliceous corals, stromatoporoids, bivalves and gastropods (Walley 1997). The outcrop of the Qartaba area had a brownish-grey color but a more brownish color for the weathered side (Fig. 2). Many carbonate samples are very firm and of micritic texture with fossils (most probably bivalves) that range in size from 0.1 to 0.5 cm. The Bikfaya Formation appears to follow on conformably from the Bhannes Formation although the existence of soil horizons in that unit suggests the potential for a time gap (Walley 1997), and is overlain by the Salima limestone which is eroded in the study area.

The Chouf Formation represents the lowest Cretaceous strata of the Lebanese stratigraphy which lies unconformably on top of the Jurassic strata. It is of Neocomian–Barremian age and varies in thickness from a few meters to 300 m throughout Lebanon (Walley 1997). This formation is composed mainly of cross-bedded, ferruginous, brown to white quartz-rich, sandstones (including shales, clays, lignites) associated with some volcanics often showing an orange, brown, hematitic color found at the base. In general, the sandstones are made up of loosely cemented quartz grains and are interbedded with marl, minor limestones, and clay beds (Nader 2000).

The Abeih Formation spans probably from Barremian to earliest Aptian and consists of alternating clastic and carbonate beds, serving as a transition between the basal Cretaceous sandstone and the overlying thick-bedded carbonates of the Mdairej Formation (Dubertret 1955, 1975; Walley 1983, 1997; Nader 2000). It shows a clear contact with the Chouf Formation, as its lowermost beds contain pisolites. More details on the regional setting and lithostratigraphy of the Lebanese rocks can be found in Nader (2014).

Methodology

Petrography and mineralogy

A total of 16 thin sections, representing the different rock types collected from the study area, were prepared for petrological study following the standard preparation processes of thin sectioning. Out of these sixteen samples, eight were selected from the Kesrouane Formation, two from the Bikfaya Formation, five from the Chouf Formation, and one from the Abeih Formation. Impregnation was particularly applied on the sandstone chips collected from the Chouf and Abeih Formations due to their high friability, where an epoxy solution was used for this purpose. Carbonate samples, on the other hand, were stained with Alizarin Red-S to differentiate between calcite and dolomite. The staining solution was prepared by adding 0.2 g of Alizarin Red-S to 100 ml of weak hydrochloric acid solution (1.5%).

Each thin section was examined properly using a light microscope with 10 × and 40 × magnification. Standard microfacies types were assigned to each sample according to Wilson (1975) and Flügel (1982). Porosity was investigated following the methods of Scholle and Ulmer-Scholle (2003), and Selley and Sonnenberg (2015). Many other features reflecting the nature of the rocks and the paleoenvironment such as grain types (bioclast vs. non-bioclast), type of porosity, effects of cement and matrix on porosity, textures (roundness, sphericity, sorting, grain size, and packing) and any diagenetic evidence were also examined. Sorting percentage is estimated following Longiaru (1987), whereas the bioclast/non-bioclast ratio is determined after Baccelle and Bosellini (1965).

To support the results of the petrographic study and to have more constraints on the rock texture and the pore system, a total of eight rock samples were investigated by the Scanning Electron Microscope (SEM) in the Central Research Science Laboratory (CRSL) at the American University of Beirut. Samples were prepared in small chips, then mounted onto copper stubs and coated with gold and carbon for optimum resolution. In addition, the simple acid-insoluble residue (AIR) analysis (Blatt 1992), which is a quick estimate of the non-carbonate percentage in the rock, was done for 23 powdered rock samples. About 10 g of the dry powdered rock is dissolved in 10% HCl acid for 24 h to ensure complete digestion of the carbonate fraction in the rock. The weight of the remaining residue is used to calculate the percentage of carbonate minerals in a given rock.

Petrophysical and elastic measurements

Petrophysical measurements were conducted on 49 rock samples; out of which 28 were from the Kesrouane Formation, seven samples from the Bikfaya Formation, ten samples from the Chouf Formation, and four samples from the Abeih Formation (Fig. 2). These specimens were cored from exposed rocks in the field. After routine core preparation (e.g., slicing and drying), the core samples were then used for various petrophysical and elastic measurements.

Rock density and porosity

Density and porosity are two key parameters affecting many of the rock characteristics. Whereas the grain density depends only on the solid constituents, the bulk density is controlled both by the grains and pores and thus reflects the compactness and cementation of the rock which will affect its overall petrophysical and elastic properties (e.g., Siegesmund and Dürrast 2014). Porosity is a fundamental measure of the storage capacity of a rock; whereas both bulk density and porosity are often related to the strength of rock material. A low-density/high-porosity rock usually has a low strength. To determine the rock porosity, we followed the Archimedes method of porosity measurement where samples are weighed successively in dry conditions, after saturation with water under vacuum, and immersed in a water tank. From the three mass measurements, one can estimate the porosity ρ, bulk density ρ_b, and grain density ρ_g. A highly porous rock will have a very small ρ_b compared to ρ_g, while a non-porous (zero porosity) rock have theoretically identical ρ_b and ρ_g. Grain density can be used to discriminate between different mono-mineralic rocks such as sandstones, limestones, and dolomites whose average grain densities are 2.64, 2.72, and 2.86 g/cm^3, respectively.

Permeability

Permeability depends on many rock parameters such as the grain size, shape, roundness, rock pore geometry, connectivity, texture, cementation, and other diagenetic processes. Rock permeability (k) was measured with a gas permeameter using nitrogen as the flowing fluid (Vinci Poro-Perm). With this device, permeability measurements are automatically corrected for the gas slippage effect (Klinkenberg 1941) as presented in Fig. 3.

Water absorption

Water absorption is another important rock index that is related to its ability to take in water and depends on the mineralogy, porosity, and pore size distribution. Water absorption is one of the key physical properties to be determined

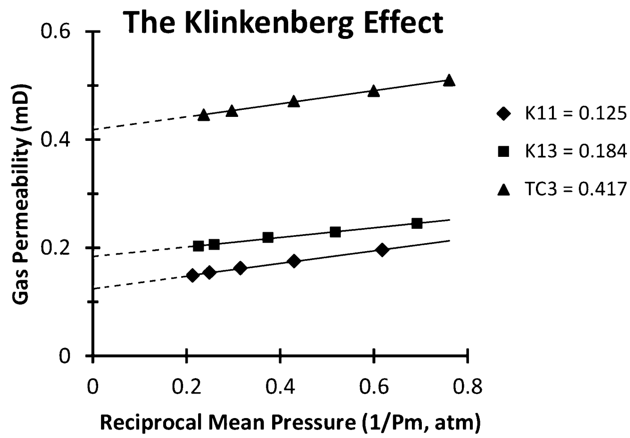

Fig. 3 The Klinkenberg correction plot for the estimation of rock permeability. Extrapolation of the straight lines intersects the vertical axis in a value which corresponds to the liquid permeability. Three samples: K11, K13, and TC3 are shown on the plot with corresponding permeabilities of 0.125, 0.184, and 0.417 mD, respectively

when evaluating the quality of rocks used as construction and building materials (e.g., Ersoy et al. 2016). The total water absorption value under atmospheric pressure conditions (W_{atm}) indicates how much water a rock can absorb over 24 h when placed 3–5 cm below the water level (Siegesmund and Dürrast 2014). The subsequent weighing of the sample wet mass (m_w, in g) and the original dry mass (m_d, g) of the sample give the water absorption according to the following equation:

$$W_{atm} = [(m_w - m_d)/m_d] \times 100(\%). \quad (1)$$

Seismic velocities

Both V_p and V_s were measured at the room temperature and under ambient pressure for the dry and water-saturated core samples using Panametrics Pulser-Receiver (Model 5058PR) and an Agilent DSO-X-2014A Digital Storage Oscilloscope (100 MHz). To ensure good coupling between the sample and the two transducers, both end surfaces of the cores were cut, and faces were polished. The first arrival time of the corresponding pulse, after passing across a sample of known length, is read on the oscilloscope with an accuracy of 0.01 µs and is used to calculate V_p or V_s. To account for the seismic anisotropy which may result from preferred alignments of rock grains or cracks, three measurements of velocity—one across the axis of the core and two perpendicular directions across diameter—were taken and the results averaged.

Poisson's ratio (σ) is the ratio between the lateral and longitudinal strains resulting from uniaxial stress applied to the rock. It is calculated from V_p and V_s using the following relation:

$$\sigma = [(V_p/V_s)^2 - 2]/2[(V_p/V_s)^2 - 1]. \quad (2)$$

This parameter varies over the range 0–0.5 for the majority of dry and saturated rocks with an average of 0.25 for the Earth's crustal rocks (Nur and Simmon 1969; Gregory 1976). Negative values of Poisson's ratio are also expected for some rocks under certain circumstances when the V_p and V_s behave differently under different rates of fluid saturation (El Sayed et al. 1998; Abuseda 2010; Boulanouar et al. 2013). The Poisson's (or V_p/V_s) ratio is very sensitive to the existence of fluids and has been used extensively as a measure of the seismogenic behavior and petrological characteristics of fluid-saturated crustal and upper mantle rocks in subduction zone settings (Zhao et al. 1996; Zhao and Negishi 1998; Nakajima et al. 2001; Salah and Zhao 2003; Salah and Seno 2008; Salah et al. 2014).

Other elastic parameters such as the bulk (κ), Young (E), and shear (G) moduli, as well as the Lame parameter (λ), can be estimated from the measured velocities and bulk density (Mavko et al. 2009). Any two of these intrinsic elastic parameters offer the basic data necessary to characterize Earth materials.

Results

The petrophysical and elastic properties of the studied rocks (measured and calculated) are listed in Tables 1 and 2, whereas the elemental chemical compositions of selected samples are given in Table 3.

Petrographic study

Eight thin sections prepared from samples collected from the Kesrouane Formation (K2, K4, K7, K8, K11, K16, K20, and K26) show distinct facies which can be divided into different groups. The first group is classified as grainstone facies according to Dunham's classification (samples K2 and K4). As seen under the microscope and confirmed by the AIR test (Table 1), samples consist essentially of carbonates (98%).

Table 1 Measured and calculated petrophysical parameters of the studied core samples

S. no.	φ	WA	ρ_b	ρ_g	k	AIR	S. no.	φ	WA	ρ_b	ρ_g	k	AIR
K1	1.95	0.70	2.77	2.82	0.006	–	K27	1.04	0.39	2.68	2.70	0.088	–
K2	3.39	1.24	2.73	2.82	0.157	1.93	K28	0.75	0.28	2.69	2.71	–	1.70
K3	1.60	0.58	2.77	2.81	0.028	–	K29	1.51	0.56	2.67	2.72	0.100	–
K4	1.46	0.53	2.78	2.82	0.031	2.20	B2	4.73	1.84	2.57	2.69	0.011	6.20
K5	2.30	0.84	2.76	2.82	0.013	–	B3	7.35	2.79	2.63	2.84	0.147	–
K6	3.55	1.30	2.73	2.83	0.025	–	B4	0.75	0.28	2.68	2.70	–	–
K7	5.18	1.95	2.66	2.81	0.068	2.00	B5	2.11	0.80	2.65	2.71	–	2.00
K8	3.31	1.21	2.72	2.82	–	2.80	B6	3.05	1.16	2.63	2.71	0.009	–
K9	2.49	0.90	2.76	2.83	0.075	–	B7	0.50	0.19	2.69	2.70	–	3.60
K10	3.30	1.23	2.69	2.78	0.033	–	B8	2.12	0.81	2.64	2.69	0.005	–
K11	4.05	1.49	2.72	2.83	0.125	3.80	TC1	23.47	11.57	2.03	2.65	***	97.88
K12	2.98	1.09	2.74	2.83	0.408	–	TC2	4.18	1.52	2.75	2.87	0.064	6.40
K13	2.58	0.94	2.74	2.81	0.184	–	TC3	4.76	1.74	2.73	2.87	0.417	–
K14	4.30	1.59	2.71	2.83	0.035	2.30	TC4	4.36	1.58	2.75	2.87	0.050	4.10
K15	2.99	1.09	2.73	2.81	0.030	–	TC5	17.58	7.66	2.29	2.78	0.660	66.70
K16	4.74	1.76	2.69	2.82	0.041	1.93	TC6	14.91	6.16	2.42	2.85	3.679	–
K17	0.21	0.08	2.79	2.80	0.032	–	TC7	11.37	4.54	2.51	2.83	1.364	46.00
K18	1.52	0.55	2.78	2.82	0.097	–	TC8	15.64	6.54	2.39	2.84	0.849	–
K19	1.34	0.48	2.79	2.83	0.013	–	TC9	8.35	3.43	2.43	2.66	2.770	76.09
K20	0.96	0.36	2.68	2.71	–	1.93	TC10	12.77	5.31	2.40	2.76	0.140	–
K22	1.11	0.41	2.68	2.71	0.004	–	TA1	6.82	2.71	2.52	2.71	0.005	58.93
K23	1.08	0.40	2.69	2.72	–	1.03	TA2	13.53	5.70	2.37	2.74	0.485	–
K24	1.33	0.49	2.68	2.72	0.002	–	TA3	9.36	3.79	2.47	2.72	0.071	61.37
K25	1.23	0.46	2.67	2.70	0.035	–	TA4	2.53	0.96	2.64	2.71	–	7.55
K26	2.73	0.99	2.77	2.84	0.043	12.25							

The three-star mark '***' denotes a broken sample; while '–' denotes either impermeable sample, or non-determined AIR

φ porosity (%), *WA* water absorption (%), ρ_b bulk density (g/cm^3), ρ_g grain density (g/cm^3), k permeability (mD), *AIR* acid insoluble residue (%)

Table 2 Measured and calculated elastic parameters of the dry and water-saturated core samples

S. no.	Dry samples							Water-saturated samples						
	V_p	V_s	G	κ	E	λ	σ	V_p	V_s	G	κ	E	λ	σ
K1	4265	2470	16.9	27.8	42.1	16.53	0.25	5969	2873	22.85	68.18	61.67	52.95	0.35
K2	2894	1511	6.20	14.5	16.3	10.37	0.31	5312	1858	9.41	64.38	26.92	58.11	0.43
K3	2096	1451	5.80	4.40	12.1	0.53	0.04	5644	3480	33.53	43.50	80.03	21.15	0.19
K4	3421	1976	10.8	18.0	27.1	10.80	0.25	6010	2663	19.70	74.04	54.27	60.91	0.38
K5	2774	1875	9.70	8.30	20.9	1.83	0.08	5735	2481	16.97	68.07	47.00	56.76	0.38
K6	4486	2827	21.8	25.8	51.1	11.27	0.17	5928	2680	19.61	69.78	53.80	56.71	0.37
K7	3327	1988	10.5	15.4	25.7	8.40	0.22	5541	2571	17.58	58.23	47.92	46.51	0.36
K8	3284	1870	9.50	16.7	24.0	10.37	0.26	6141	2772	20.92	74.82	57.41	60.87	0.37
K9	2185	1383	5.30	6.10	12.3	2.57	0.17	5060	1947	10.47	56.78	29.60	49.80	0.41
K10	3014	1947	10.2	10.8	23.3	4.00	0.14	5793	2543	17.42	67.14	48.10	55.53	0.38
K11	2901	1630	7.20	13.2	18.3	8.40	0.27	6001	2426	15.99	76.54	44.86	65.88	0.40
K12	1725	1221	4.10	2.70	8.20	− 0.03	0.00	5249	1648	7.45	65.62	21.53	60.65	0.45
K13	2456	1287	4.50	10.5	11.9	7.50	0.31	5388	2012	11.10	64.77	31.49	57.37	0.42
K14	–	1404	5.30	–	–	–	–	5500	2082	11.75	66.37	33.29	58.54	0.42
K15	3015	1720	8.10	14.1	20.3	8.70	0.26	5717	2330	14.82	69.48	41.51	59.60	0.40
K16	4198	2355	14.9	27.5	37.9	17.57	0.27	6023	2688	19.43	71.66	53.45	58.71	0.38
K17	3841	2376	15.8	20.2	37.5	9.67	0.19	6010	2772	21.47	72.31	58.60	58.00	0.36
K18	3175	1933	10.4	14.2	25.0	7.27	0.21	6054	2491	17.25	78.87	48.22	67.37	0.40
K19	3024	1779	8.80	13.7	21.8	7.83	0.24	5957	2580	18.58	74.25	51.45	61.86	0.38
K20	6400	3263	28.5	71.7	75.5	52.70	0.32	6422	3328	29.67	70.93	78.13	51.15	0.32
K22	6373	3196	27.3	72.2	72.8	54.00	0.33	6315	3299	29.12	67.89	76.42	48.48	0.31
K23	6271	3232	28.1	68.3	74.1	49.57	0.32	6296	3092	25.69	72.28	68.91	55.15	0.34
K24	6360	3173	27.0	72.6	72.1	54.60	0.33	6377	3285	28.96	70.55	76.43	51.24	0.32
K25	6254	3178	26.9	68.4	71.5	50.47	0.33	6302	3286	28.81	67.57	75.68	48.36	0.31
K26	2772	1802	9.00	9.30	20.4	3.30	0.13	5575	2245	13.94	67.37	39.13	58.08	0.40
K27	6361	3176	27.0	72.3	72.0	54.30	0.33	6403	3172	26.92	73.80	72.01	55.85	0.34
K28	6283	3190	27.3	69.6	72.5	51.40	0.33	6342	3188	27.30	71.65	72.67	53.45	0.33
K29	6259	3221	27.7	67.8	73.2	49.33	0.32	6259	3045	24.80	71.68	66.71	55.15	0.34
B2	5130	2839	20.7	40.0	52.9	26.20	0.28	5467	2772	19.72	50.42	52.34	37.27	0.33
B3	4045	2360	14.7	23.5	36.4	13.70	0.24	4821	2245	13.26	43.46	36.11	34.62	0.36
B4	6273	3192	27.3	69.1	72.5	50.90	0.33	6344	3278	28.84	69.55	76.00	50.32	0.32
B5	6128	3173	26.7	64.0	70.3	46.20	0.32	5955	3016	24.13	61.92	64.07	45.83	0.33
B6	5748	2962	23.1	56.1	60.9	40.70	0.32	5929	2922	22.45	62.47	60.15	47.50	0.34
B7	6455	3222	27.9	74.8	74.4	56.20	0.33	6373	3027	24.62	76.30	66.68	59.89	0.35
B8	5915	3035	24.3	59.8	64.1	43.60	0.32	5965	2867	21.67	64.87	58.49	50.42	0.35
TC1	–	984	2.00	–	–	–	–	2386	–	–	–	–	–	–
TC2	3804	2333	15.0	19.8	35.9	9.80	0.20	4898	2311	14.69	46.39	39.86	36.60	0.36
TC3	3464	2167	12.8	15.7	30.2	7.17	0.18	4484	1833	9.18	42.67	25.70	36.55	0.40
TC4	4086	2413	16.0	24.6	39.5	13.93	0.23	5295	2386	15.66	56.22	42.98	45.78	0.37
TC5	3496	1799	7.40	18.1	19.6	13.17	0.32	4176	1875	8.06	29.26	22.15	23.89	0.37
TC6	2981	1724	7.20	11.9	18.0	7.10	0.25	3620	1646	6.56	22.99	17.97	18.62	0.37
TC7	3797	2111	11.2	21.2	28.5	13.73	0.28	4348	1939	9.43	34.81	25.94	28.52	0.38
TC8	3015	1799	7.70	11.4	18.9	6.27	0.22	3600	1691	6.84	21.89	18.59	17.33	0.36
TC9	4369	2477	14.9	26.6	37.7	16.67	0.26	4892	2661	17.24	35.26	44.47	23.77	0.29
TC10	4072	2491	14.9	20.0	35.8	10.07	0.20	4370	2287	12.58	29.15	32.98	20.76	0.31
TA1	4553	2611	17.2	29.4	43.2	17.93	0.26	4840	2592	16.96	36.49	44.05	25.18	0.30
TA2	3482	2046	9.90	15.5	24.6	8.90	0.24	3879	1850	8.12	24.89	21.98	19.48	0.35
TA3	4402	2593	16.6	25.7	41.0	14.63	0.23	4660	2439	14.68	34.02	38.51	24.23	0.31
TA4	5752	3040	24.4	54.8	63.8	38.53	0.31	5965	2989	23.61	62.54	62.92	46.80	0.33
Min	1725	984	2.00	2.70	8.2	− 0.03	0.08	2386	1646	6.56	21.89	17.97	17.33	0.19
Max	6455	3263	28.5	74.8	75.5	56.2	0.33	6422	3480	33.53	78.87	80.03	67.37	0.45
Avg	4263	2323	15.4	32.3	40.6	21.67	0.25	5461	2572	18.33	58.83	49.36	46.62	0.36

The '–' denotes unreliable waveform and poor arrival time picking

V_p primary wave velocity (m/s), V_s secondary wave velocity (m/s), G shear modulus, κ bulk modulus, E Young's modulus; λ Lame parameter (elastic moduli are given in GPa), σ Poisson's ratio

Table 3 The elemental chemical composition of selected samples

Sample	Chemical composition							
	C %	O %	Mg %	K %	Ca %	Fe %	Si %	Al %
K4	15.02	56.21	13.43	0.73	14.61	0	0	0
K16	15.95	36.56	13	0	34.49	0	0	0
B7	8.98	45.09	0	0	45.92	0	0	0
TC1	14.8	41.14	0	0	0	0	44.05	0
TC2	17.45	45.5	9.72	0	22.53	4.8	0	0
TA3	12.35	49.23	0.8	0	0.85	3.96	30.15	2.66

The SEM analysis revealed that the samples are composed of 70–80% dolomite grains and 10–20% calcite where carbon, calcium, and magnesium concentrations are very high (sample K4, Table 3). Samples of this facies are well compacted (Fig. 4a) with very low intergranular primary porosity (~ 1 to 2%; Fig. 4b) as well as minor secondary fracture porosity (1%). Some calcite veins are observed in sample K4 due to dissolution and secondary precipitation (Fig. 4c). Middle to outer shelf is, most probably, the depositional environment of this group of rocks.

The second facies recognized in the Kesrouane Formation is made up of dolomitic grainstone (samples K7, K8, K11, and K16) but with a significant increase in the proportion of calcite grains as revealed by the SEM analysis (sample K16, Table 3). The AIR test indicates that samples are also composed mainly of carbonates (Table 1). Dolomite crystals are generally planar and euhedral with a size of 2500 µm (Fig. 4d). These crystals form a hypidiotopic mosaic with straight comprise boundaries. Both the primary and secondary porosities of this group are low (3–5%) due to the high compaction (Table 1; Fig. 4e, f). Highly reworked fossils such as foraminifera and bone fragments are present (Fig. 4g–i), while veins are absent. Samples belonging to this group are dolomitic limestones that were deposited in a shallow water setting.

The third facies found in this formation was detected in samples K20 and K26 and is classified as micritic limestone/mudstone according to Folk's classification (sample K20, Fig. 4j). This facies is mud-supported and composed essentially of 90% calcite grains with some oxide minerals. The AIR test shows that sample K20 consists of 98% carbonates. This sample contains fossils as foraminifera and ostracods (Fig. 4j, k). It is characterized by very low primary intergranular (0.5%) and fractured (1%) porosity with some calcite veins (Fig. 4l), which are consistent with the measured porosity (Table 1). This facies was deposited in an outer shelf environment.

Two thin sections were prepared from the limestone samples (samples B2 and B7) taken from the Bikfaya Formation. Under the microscope, the thin sections are dominated by calcite with a minor amount of quartz (Fig. 4m–p), which were also observed in the SEM analysis (Table 3). Grains of calcite with rhombohedral cleavage are visible in sample B2 (Fig. 4m). The AIR test shows that the two samples are made up of more than 93% carbonates (Table 1). Veins and small fractures are detected, indicating the extensional forces affecting these beds. The veins are partially filled also by calcite grains (Fig. 4n). Furthermore, fossils such as ostracods (Fig. 4o), ammonoids (Fig. 4p), foraminifera (Fig. 5a), bone fragments and echinoids (Fig. 5b), are abundant in sample B7 but absent in sample B2. Primary porosity, accordingly, is expected to be very low (Table 1). Secondary porosity resulted mainly from fracturing and dolomitization (Fig. 5c, d) and dissolution of fossils (Fig. 5d). Sample B2 is classified, according to Dunham's classification, as wackstone to packstone while sample B7 as crystalline wackstone. These samples were deposited in a middle shelf to near shore depositional environment.

The petrographic study of the rocks taken from the Chouf Formation (TC1 to TC10) reveal that the rocks are essentially quartzarenites (ferruginous sandstones) intercalated with limestones and dolomites. The SEM and thin section investigations show that sample TC1 is composed essentially of 90–95% quartz with traces of feldspars and a little percentage of iron oxides (Table 3). The AIR test indicates that this sample is made mostly of non-carbonate components (97.88%, Table 1). Quartz grains have a medium degree of maturity due to their subangular/subrounded nature and medium sorting (Fig. 5e–g). Voids are found between grains giving a primary (intergranular) porosity of 20–25% (an estimate that is verified by the results listed in Table 1). Under the microscope, there is a high intergranular porosity with no secondary porosity (Fig. 5f, g). This type of sandy facies is deposited in a continental margin where the sea level is low. In this environment, the kinetic energy varies from moderate to high resulting in the high friability of the samples. Sample TC2 consists of 20% dolomite and 70% calcite with no fossils as seen under the microscope and reported in the SEM analysis (Table 3; Fig. 5h). It has up to 94% carbonate components (Table 1). The sample is characterized by both primary (intergranular) porosity (3.2%) and secondary (fractured and intragranular) porosity (2%; Fig. 5i). Partially filled calcite veins are also seen (Fig. 5j).

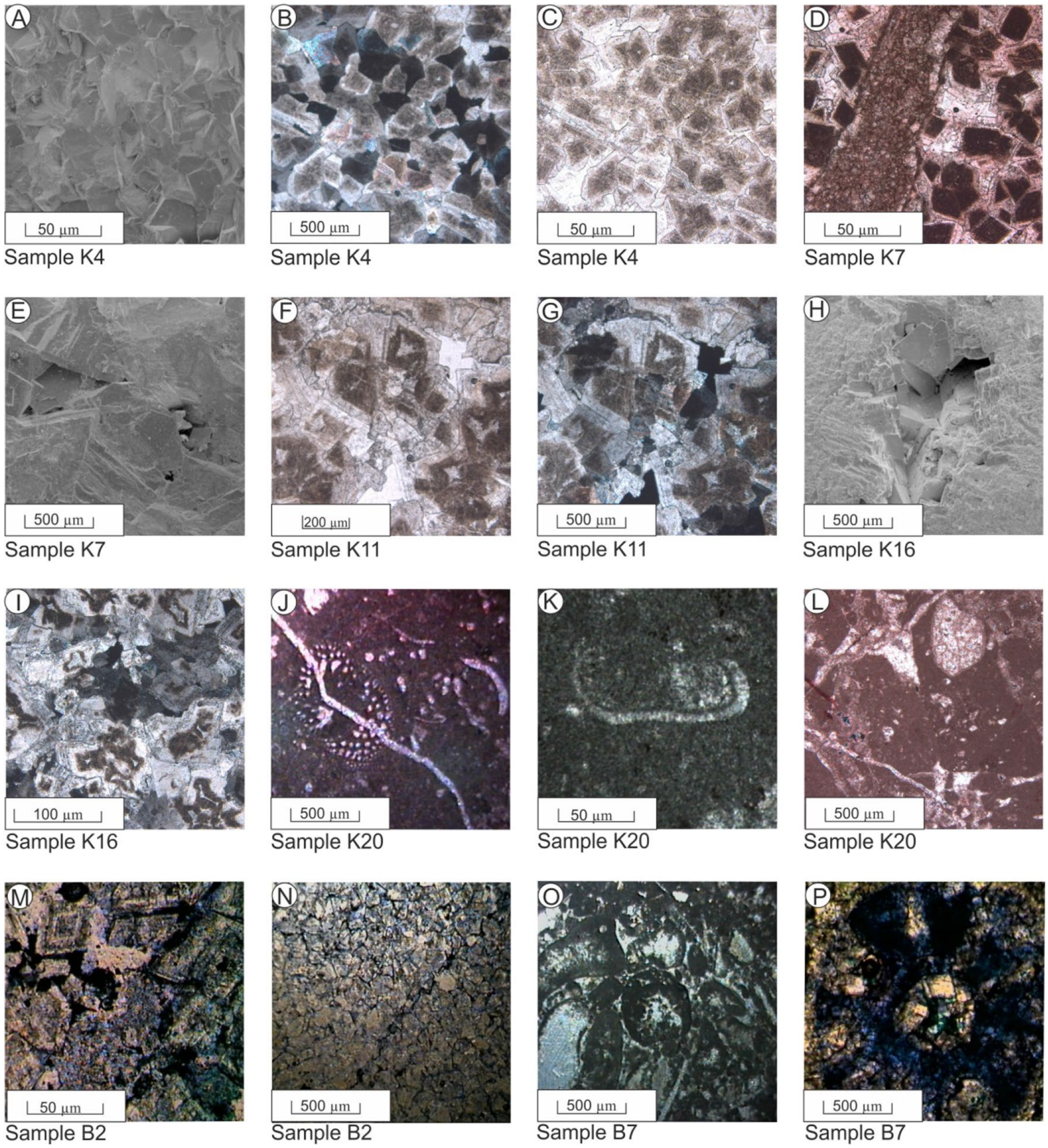

Fig. 4 Scanning electron microscopy and thin section photomicrographs of representative samples collected from the studied area. **a** Well compacted interlocking crystals, **b** low primary intergranular porosity, **c** secondary precipitation of calcite, **d** euhedral dolomite crystals, **e**, **f** low primary and secondary porosity, **g**, **h** reworked fossils, **i** compact grainstone, **j**, **k** foraminifera and ostracods, **l** calcite veins, **m** rhombohedral cleavages, **n** veins partially filled by calcite, **o** fossils remains and **p** ammonoids. Sample number is shown below each image, whereas the scale bar is shown to the lower left

This sample is classified as dolomitic limestone which was deposited in a shallow marine environment. Sample TC3 is made up mostly of dolomite with minor calcite and some quartz (Fig. 5k). Iron oxide matrix partially fills the pore spaces between the dolomite grains. This sample is classified as a grainstone due to the dominance of the rhombic-shaped dolomite grains and the less matrix (less than 10%). Intragranular porosity in the sample resulted from the secondary substitution between calcium and magnesium. Samples TC6 and TC10 are made up mostly of quartz without any fossils. In addition, wollastonite and some other minerals are also detected. Sample TC6, in particular, is characterized by a high primary porosity of 15.0% (Fig. 5l), whereas sample TC10 exhibits a sieve texture (Figs. 4n, 5m) which enhances the primary intergranular porosity to 13%, but with no secondary porosity.

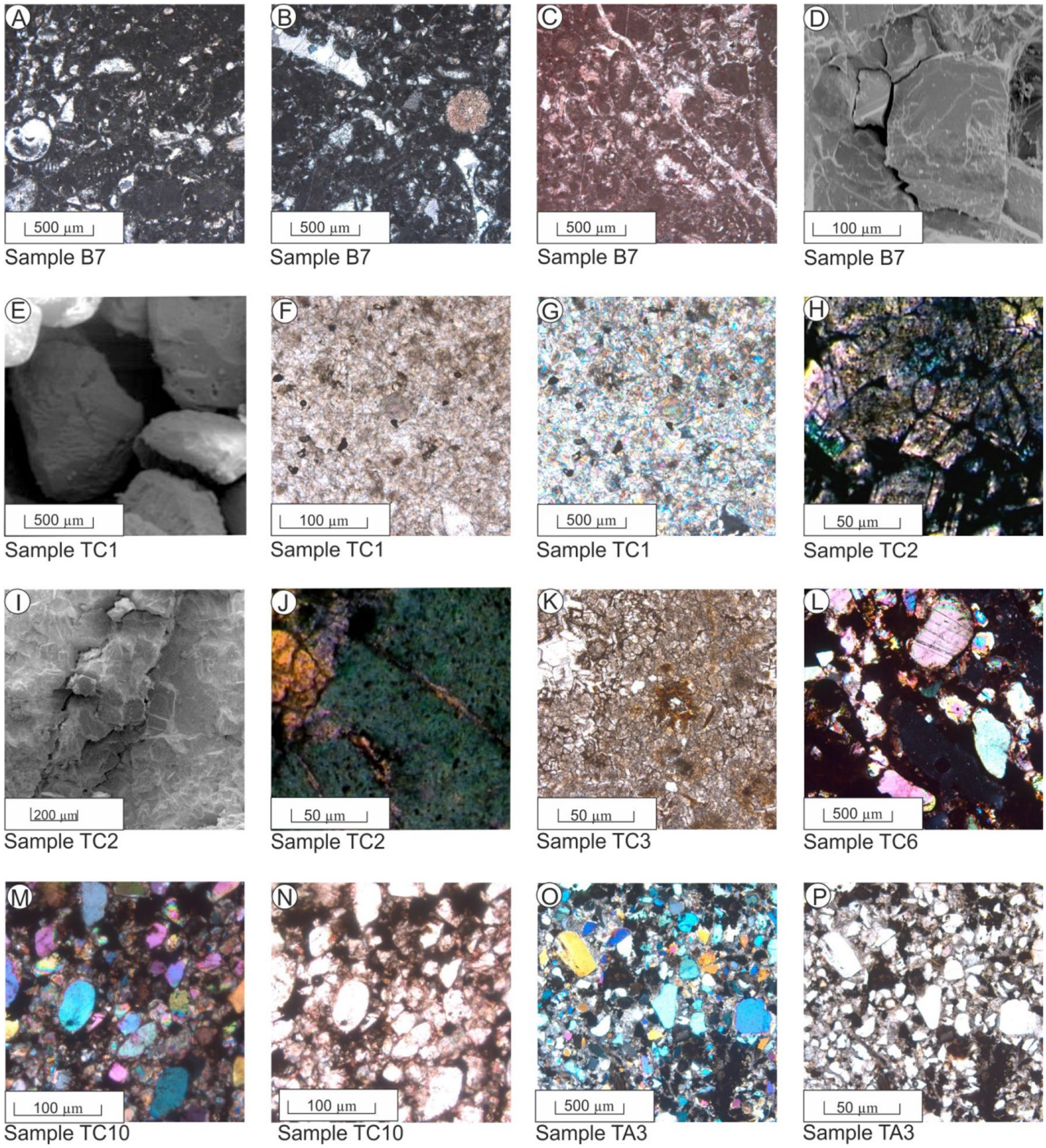

Fig. 5 Scanning electron microscopy and thin section photos of representative samples collected from the studied formations. Fossils foraminifera (**a**), bone fragment (**b**), and echinoids (**c**), fractured porosity (**d**), subrounded quartz grains with high intergranular primary porosity (**e**–**g**), dolomite and calcite crystals (**h**), fractured and intragranular porosity (**i**), partially filled calcite veins (**j**), sieve texture (**k**), iron oxide-cemented sandy limestone (**l**), poor to moderately sorted sandstones facies with moderate porosity and various types of cements (**m**–**p**). Sample number is shown below each image, whereas the scale bar is shown to the lower left

Sample TC10 is characterized by its calcite and quartz content (Fig. 5n) with perhaps other minerals. The two samples TC6 and TC10 are classified as shallow marine calcareous sandstones that were deposited in conditions of moderate to high kinetic energy.

The thin section prepared from the Abeih Formation (TA3) is characterized by its high quartz content with other minerals enriched in aluminum and iron oxides embedded in a carbonate matrix (Fig. 5o, p), which is also verified by the SEM analysis (Table 3). In addition, the AIR test shows that this sample contains up to ~ 61.5% non-carbonate constituents (Table 1). Moreover, it is characterized by heterogeneous porosity (Fig. 5o). The sample has an overall porosity of 2% (secondary) and 9% (primary) as shown in the table and emphasized by the microscopic examination and the SEM investigation (Fig. 5o). Results of the XRD analysis revealed that calcite, dolomite, and quartz are the dominant minerals (Fig. 6). In addition, minor amounts of clays, iron oxides, and feldspar are also encountered.

Petrophysical characteristics and interrelationships

Porosity is the most critical parameter of a rock affecting all of its physical and elastic properties. It also controls the permeability as it provides the space and pathways for fluids to flow through rocks. A high porosity of rock usually leads to high permeability unless the pores are of small sizes or connected by very narrow pore throats. The majority of the samples in our study have very low porosity (average 4.8%), which can be classified as negligible to poor porosity (e.g., Eysa et al. 2016). Although porosity varies from 0.21 to 23.47%, only ten samples (mainly from the Chouf and Abeih Formations) have porosities greater than 10% (moderate porosity), and 12 samples have porosities greater than 5%, implying that 37 samples (mainly carbonates) have lower-than-5% porosity (Table 1). The moderate-porosity samples are mainly the sandstones (also some sandy dolomites and sandy limestones) of the Chouf and Abeih Formations. In addition, water absorption (which is strongly related to porosity) is very low for the carbonate samples but moderate for the sandstones. The minimum values are observed for the compact limestones of the Kesrouane Formation (e.g., sample K20) whereas the maximum is observed for the sandstones of the Chouf Formation (sample TC1; Table 1). The bulk density is generally moderate to high where it varies from 2.03 to 2.79 g/cm^3 with an average of 2.64 g/cm^3, which is very close to the typical grain density of sandstone. These moderate/high bulk density data reflect the cementation and strong compaction, which lowered the porosity of the studied rocks. The grain density is also high and varies between 2.65 and 2.87 g/cm^3, with an average of 2.77 g/cm^3. Permeability of the studied rocks is generally very low to low with an average of 0.31 mD and varies between 0.002 and 3.679 mD. The majority of the compact carbonate samples of the Kesrouane and Bikfaya Formations have even permeabilities in the range of few micro Darcys; whereas only three sandstone samples from the Chouf Formation have permeabilities of very few milli Darcys (Table 1).

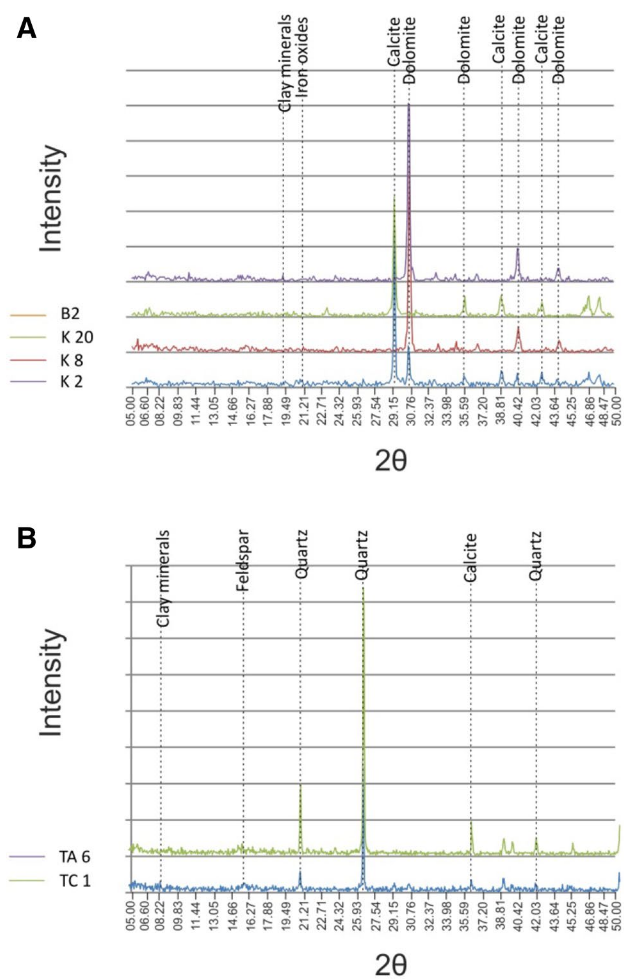

Fig. 6 Results of the XRD analysis of some samples: Calcite-dolomite group from Kesrouane and Bikfaya formations (**a**), and siliciclastics of Chouf and Abeih formations (**b**)

The studied rocks exhibit wide variations in seismic wave velocities. The V_p varies from 1725 to 6455 m/s with an average of 4263 m/s; whereas the V_s varies from 984 to 3263 m/s with an average of 2323 m/s. The average values of V_p and V_s yield a high V_p/V_s ratio of 1.84. Poisson's ratio varies also widely from 0.08 to 0.33, with an average of 0.25. Only one sample (K12) has a σ ratio of 0.0, possibly due to its unreliable V_p value. The four elastic coefficients of G, κ, E, and λ also vary widely as a result of the wide V_p and V_s variations (Table 2). In the following, we construct and discuss some interrelationships between the measured parameters.

Upon saturation, there is a considerable increase of V_p for all samples except three (Table 2; Fig. 7a). On the other hand, the V_s displays a mixed behavior where some samples witnessed a decrease in their V_s relative to the dry samples while others have higher V_s at saturation conditions (Fig. 7b). However, both V_p and V_s have higher averages after saturation. Both the rigidity and Young's modulus showed variable behavior with saturation (Table 2; Fig. 7c, e). The bulk modulus and the Poisson's ratio are also higher after saturation for the majority of samples (Fig. 7d, f).

Bulk density–porosity relationship

The relationship between φ and ρ_b is routinely investigated to give a quick check on the reliability of the measurements (Nabawy and David 2016) and can also be used as an immediate way for porosity prediction in reservoir rocks (Nabawy and Barakat 2017). Generally, the plot between the two parameters

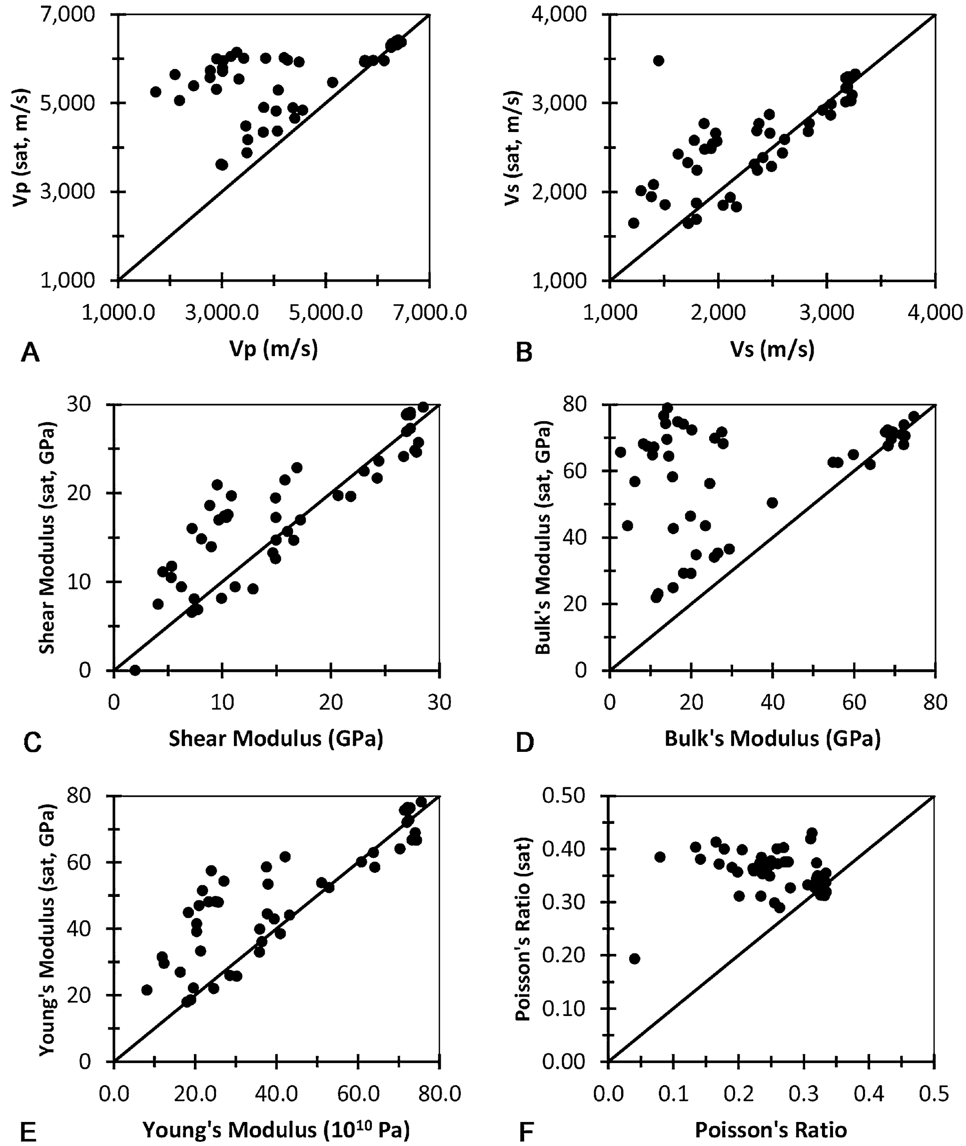

Fig. 7 The relationship between the acoustic velocities and elastic moduli of the dry and water-saturated samples (see text for more details)

displays porosity-dependent decreasing function of density (e.g., Han and Batzle 2004; Wang et al. 2009a). Figure 8a displays this inverse relationship where the increase in φ is accompanied by a decrease in ρ_b. Two clear trends (both with the same high R^2) can be easily recognized on the plot which possibly reflect different levels of compaction, cementation, or fine component content and, in turn, characteristic porosity-density dependence. Under the microscope, we did not observe any bias of certain types of lithofacies toward a particular cluster. However, most of the sandstone samples and the carbonates with high clastic ratios belong to the lower group (shown as black squares in Fig. 8a).

Porosity vs. grain density

The grain density is strongly related to lithology. The plot of grain density and porosity (Fig. 8b) reveals some important conclusions. Two clusters with different grain densities and very low porosities exist on the left reflecting the calcareous and dolomitic nature of the majority of the investigated rocks. From these two clusters, weak positive trends extend toward moderate porosities indicating that replacement of original constituents by heavier components (e.g., dolomitization and cementation with iron oxides) is accompanied by volume liberation and slight porosity enhancement. In this way, some calcareous and dolomitic sandstones have moderate porosity (of a secondary origin) and high grain density. Only two samples have grain densities of about 2.65 g/cm^3, which are almost pure sandstones (samples TC1 and TC9) but different porosities resulting from different cements and clay content. Sample TC9 is enriched in iron oxide cements, whereas TC1 is less likely cemented and, therefore, has a high porosity of 23.5%.

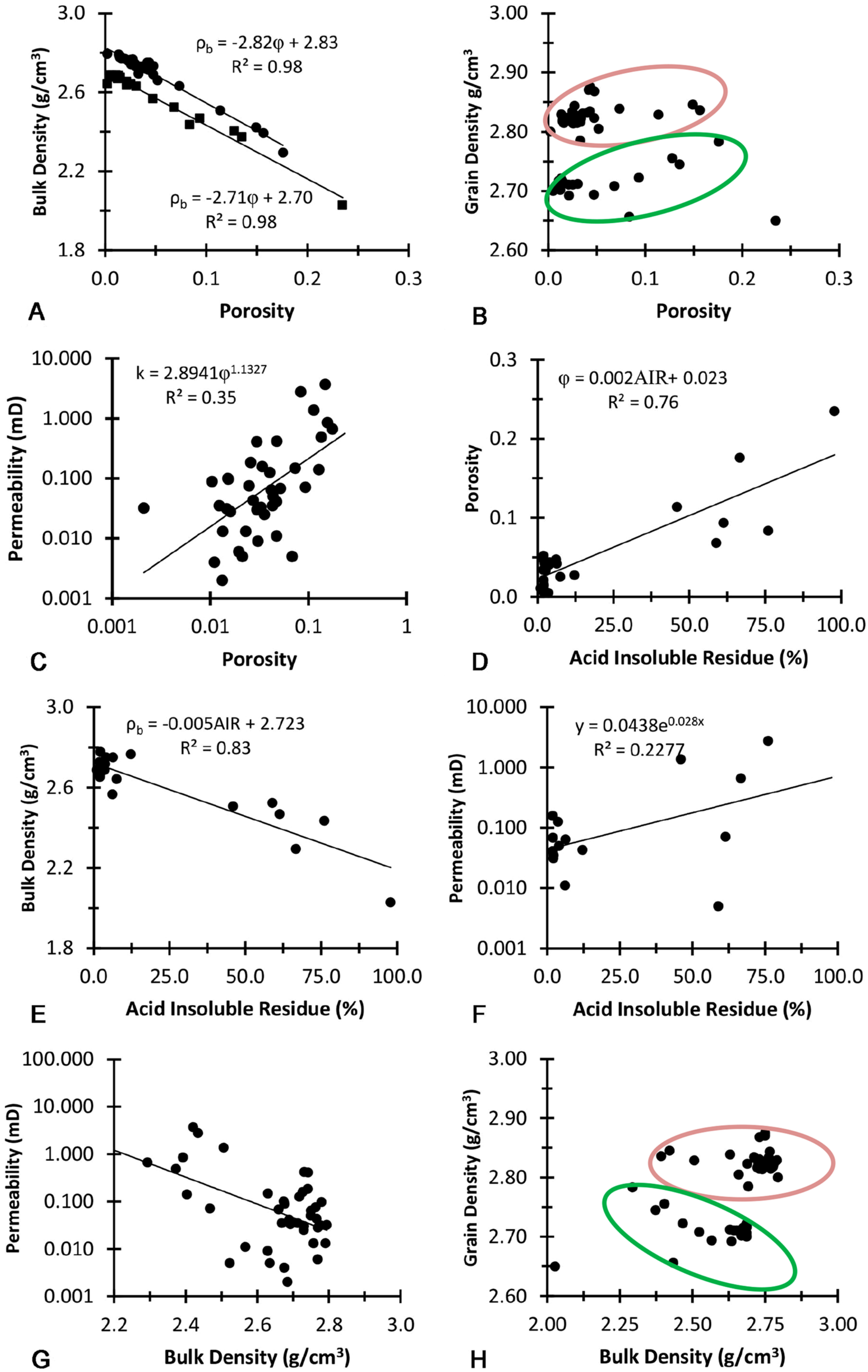

Fig. 8 Crossplots between the measured petrophysical parameters: φ vs. ρ_b (**a**), φ vs. ρ_g (**b**), φ vs. k (**c**), AIR vs. φ (**d**), AIR vs. ρ_b (**e**), AIR vs. k (**f**); ρ_b vs. k (**g**), and ρ_b vs. ρ_g (**h**)

Porosity–permeability relationship

Figure 8c illustrates the log–log relationship between porosity and permeability. Although a clear positive trend is obtained; there is a wide scatter in the plot with a fair coefficient of correlation ($R^2=0.35$). This poor poro-perm relationship is common in carbonate rocks implying that porosity is not the only parameter affecting permeability and that factors such as the grain size distribution, pore shape, pore geometry, pore throat size, cement, and mineral composition are other controlling parameters (e.g., Beard and Weyl 1973; Swanson 1981; Schmoker et al. 1985; Lucia 1995; El Sayed et al. 2015).

AIR vs. φ, ρ_b, and k

Because we have both carbonate and siliciclastic rock samples, we conducted the AIR test which supported the fact that the majority of the studied rocks are carbonates with few sandstone samples (Table 1). The AIR data exhibit direct and inverse relationships with φ and ρ_b, respectively (Fig. 8d, e) with moderate correlation coefficients ($R^2=0.76$ and 0.83), implying that there is a tendency for the clastic rocks to be more porous and less dense than the compact carbonate rocks.

The direct trend of the relationship between the AIR and permeability (Fig. 8f) also confirms the relatively higher permeability of the sandstones and the clastic-rich rocks relative to the pure carbonates. However, the small correlation coefficient results mainly from a very-low-permeability dolomitic sandstone sample (TA1, Table 1) due to the iron oxide and dolomite secondary precipitations. Sandstones may also exhibit low porosity and permeability due to intense compaction, abundant matrix, or due to specific pore spaces (Zhang et al. 2017).

Bulk density–permeability relationship

The plot of ρ_b vs. k (Fig. 8g) displays an inverse trend, although with a considerable scatter, implying that the carbonate rocks with higher bulk density are less permeable than the less dense sandstones. In addition, secondary precipitation of cementing material increases the bulk density and reduces the permeability of the majority of the studied rocks.

Bulk density vs. grain density

Whereas the bulk density reflects the rock composition and its pores, the grain density reflects the rock mineralogy. The relationship between these two related parameters can discriminate between the mineralogy of the studied rock samples based on the grain density values (Fig. 8h). The presence of iron oxide cement or other heavy minerals in sandstones may also shift their grain densities to higher values (Nabawy et al. 2015; Nabawy and Barakat 2017). Two clusters appear on the plot as seen also in the plot of porosity and grain density (Fig. 8b). The close ρ_b and ρ_g data for many samples (Fig. 8h) reflect the overall low porosity of the investigated rocks.

V_p–V_s relationships

The relationship between V_p and V_s is strongly positive (the thin solid line in Fig. 9a) with a high correlation coefficient ($R^2=0.96$) which reveals consistent velocity measurements and that V_s can be accurately predicted from the more easily measured V_p. This linear relationship between V_p and V_s is in agreement with other results (e.g., Wang et al. 2009a). It is well known that for dry, perfectly elastic, crustal rocks, $V_s=0.58V_p$ (e.g., Burger et al. 2006) which is shown by the thick solid line in Fig. 9a. Although some samples possess relatively higher shear wave velocities at low-velocity ranges, most of our samples plot well below this line implying relatively lower V_s values. The average V_p and V_s values of 4263 and 2323 m/s, respectively, for our samples, give a high V_p/V_s ratio of 1.835 (i.e., $V_s=0.54V_p$) for the studied rocks.

The overall V_s reduction relative to V_p in sedimentary rocks may be produced by porous, wet, or clay-rich rocks and, therefore, Castagna et al. (1985) proposed the so called 'Castagna mudrock equation' which precisely relates V_s to V_p in porous and wet rocks. However, because most of the samples in our study are limestones and dolomites, our plot between V_p and V_s is also compared with the empirical relationship: $V_s=V_p/1.9$ of Pickett (1963), which is characteristic for limestones (dashed line in Fig. 9a). The Pickett's model fits our data better at intermediate and higher velocities (Fig. 9a).

The V_p/V_s (or the Poisson's) ratio is becoming a more useful parameter in the determination of rock properties. The relationship between V_p and V_p/V_s is generally linear (Fig. 9b); however, some samples, especially at intermediate and to a less extent low V_p values, display a clear scatter with higher or lower V_p/V_s ratios. These samples are mostly crystalline grainstones or sandy dolomites whose shear wave velocities are more strongly impacted by more porous and complicated fabric of the low/moderate velocity carbonate rocks (Anselmetti and Eberli 1993). In stiff rocks with high V_p, the V_p/V_s ratio is also high (between 1.8 and 2.0) and no scatter was observed (Fig. 9b).

ρ_b vs. V_p and V_s

Because bulk density is strongly dependent on porosity, velocity also shows a good correlation with bulk density.

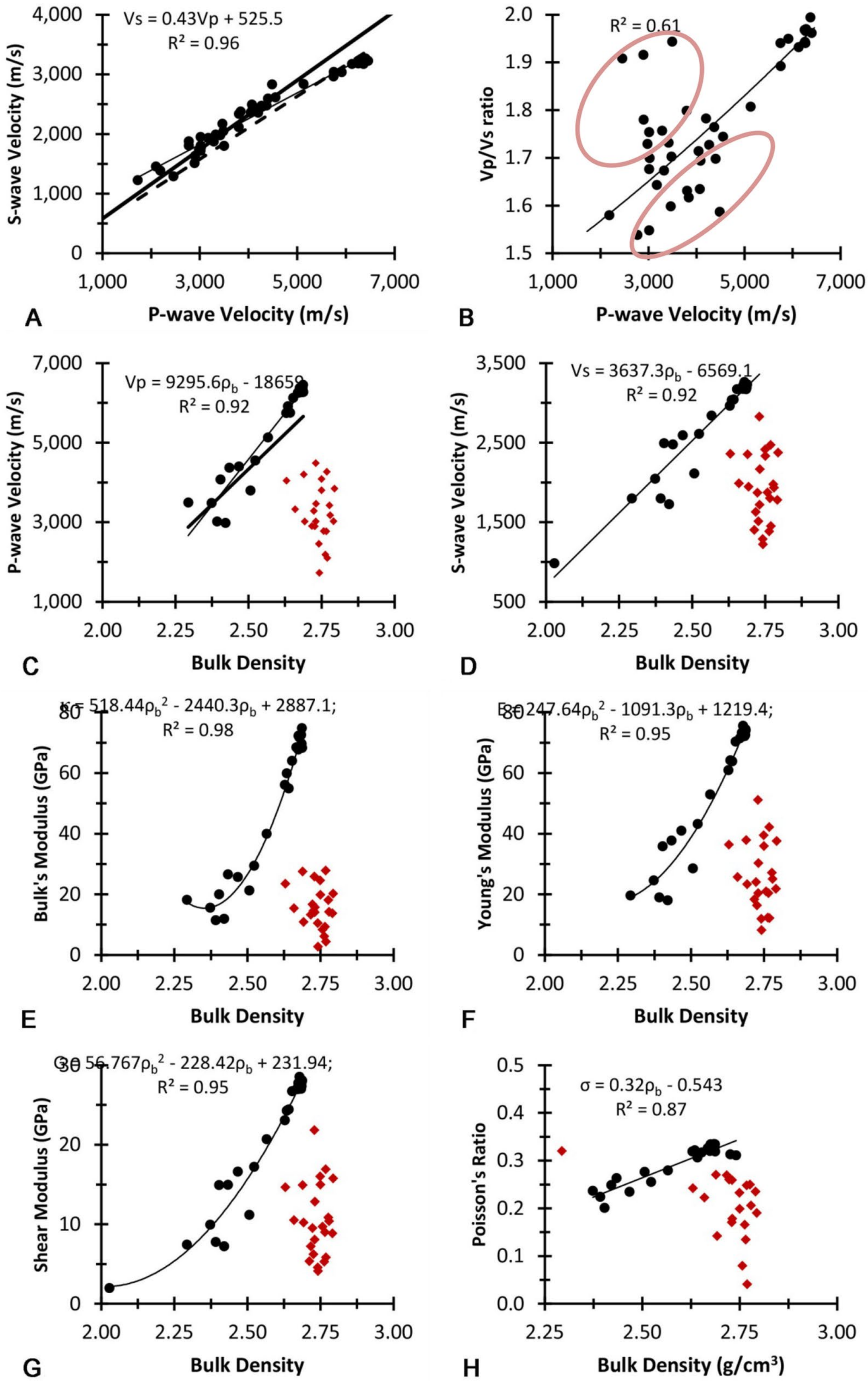

Fig. 9 Crossplots between the measured petrophysical parameters: V_p vs. V_s (**a**), V_p vs. V_p/V_s (**b**), ρ_b vs. V_p (**c**), ρ_b vs. V_s (**d**), ρ_b vs. κ (**e**), ρ_b vs. E (**f**), ρ_b vs. G (**g**), and ρ_b vs. σ (**h**)

The relationship between ρ_b and V_p usually displays a direct trend implying a greater propagation velocity in compact rocks, which is clear in Fig. 9c, where many samples are linearly aligned with a high correlation coefficient ($R^2=0.92$). The linear trend is compared to Gardner's et al. (1974) equation for sedimentary rocks: V_p (km/s) = $(\rho_b/1.74)^4$, which is valid for velocities in the range 1.5–6.1 km/s (thick solid line in Fig. 9c). Although Gardner's et al. equation is valid mainly for siliciclastic rocks, there is a minor difference between the two trends implying the robustness of our proposed linear fit. Some samples deviate clearly from this trend and exhibit lower and moderate V_p data even though their bulk densities are high and do not vary largely. These outliers are mainly the limestones of the Kesrouane Formation as well as few samples from the Bikfaya Formation with specific pore types. The same behavior is also observed for the relationship between bulk density and the shear wave velocity (Fig. 9d). It is thought that the observed deviations are induced mainly by the nature of the pore system and porosity types of these rocks as will be discussed in later sections.

Bulk density vs. elastic moduli

The relationships between ρ_b and the elastic coefficients (κ, E, G, and σ) display direct trends with moderate/high correlation coefficients (Fig. 9e–h). The elastic constants are calculated from the seismic wave velocities and the bulk density. Therefore, samples deviating from the general positive trends between bulk density and seismic wave velocities are also seen in the plots of ρ_b versus the elastic moduli of the studied rocks.

Porosity vs. seismic wave velocities and elastic moduli

Investigating the relationship between porosity and the seismic wave velocities (Fig. 10a, b) reveals that V_p and V_s decrease generally with increasing φ and that the studied samples are separated into two groups. One, as expected, exhibits clear inverse trends with high correlation coefficients where the increase in porosity is accompanied by a corresponding decrease in seismic wave velocities. The second category of samples exhibits variable velocity data at low porosities. These are the same outliers deviating from the direct ρ_b—velocity trends.

Because the elastic constants control the propagation velocity of the seismic waves, we also expect to have the two categories of samples in the plots of porosity versus the elastic moduli (Fig. 10c–e). Exponential or polynomial relationships with high correlation coefficients express the variations of the elastic coefficients with φ. The relationship between porosity and Poisson's ratio, on the other hand, displays a negative trend which means that the sandstones and the carbonate rocks having a significant clastic component, with their higher porosities, have lower Poisson's ratios compared to the pure carbonate rocks (Fig. 10f).

Permeability vs. V_p and V_s

Although the relationships between permeability and the seismic wave velocities display generally a cloud of points (e.g., El Sayed et al. 2015); an inverse trend is shown by our samples (Fig. 10g, h). Very-low permeability rocks have high V_p and V_s, and there is a gradual decrease in the acoustic velocities with the slight increase in permeability.

Porosity and bulk density vs. acoustic velocities of the water-saturated samples

The V_p of the water-saturated samples is inversely and directly correlated with porosity and bulk density, respectively (Fig. 11a, c). In contrast to the data of the dry rocks, the outliers having low velocity at lower porosities and high bulk density are not seen on the plot. On the other hand, they are recognized on the plots of V_s versus porosity and bulk density (Fig. 11b, d). Moreover, two parallel linear trends between ρ_b and V_s can be recognized with a third group of samples having low V_s at relatively high ρ_b values (Fig. 11d).

Discussion

Lithology and the elastic properties

The different depositional lithologies can sometimes explain the different ranges of the velocity data in different types of sediments. However, previous studies have shown that lithology has a minor effect on velocity in carbonate deposits (e.g., Anselmetti and Eberli 1993). In addition, Ündül (2016) did not observe a clear relationship between the mass fractions of minerals and Poisson's ratio. The minimal influence of mineralogy on velocity in carbonates can be partially explained by the small velocity contrasts of the two dominant carbonate minerals: calcite (6500 m/s) and dolomite (6900 m/s). On the other hand, the percentage of the large grains to the fine matrix has a remarkable effect on the Poisson's ratio and the other elastic properties of the rocks. For example, Poisson's ratio decreases with the increase of the fine matrix or groundmass in igneous rocks and increases with the size heterogeneity of the grains composing the rock (Ündül et al. 2015). Micritic limestones from the Kesrouane and Bikfaya Formations have generally high

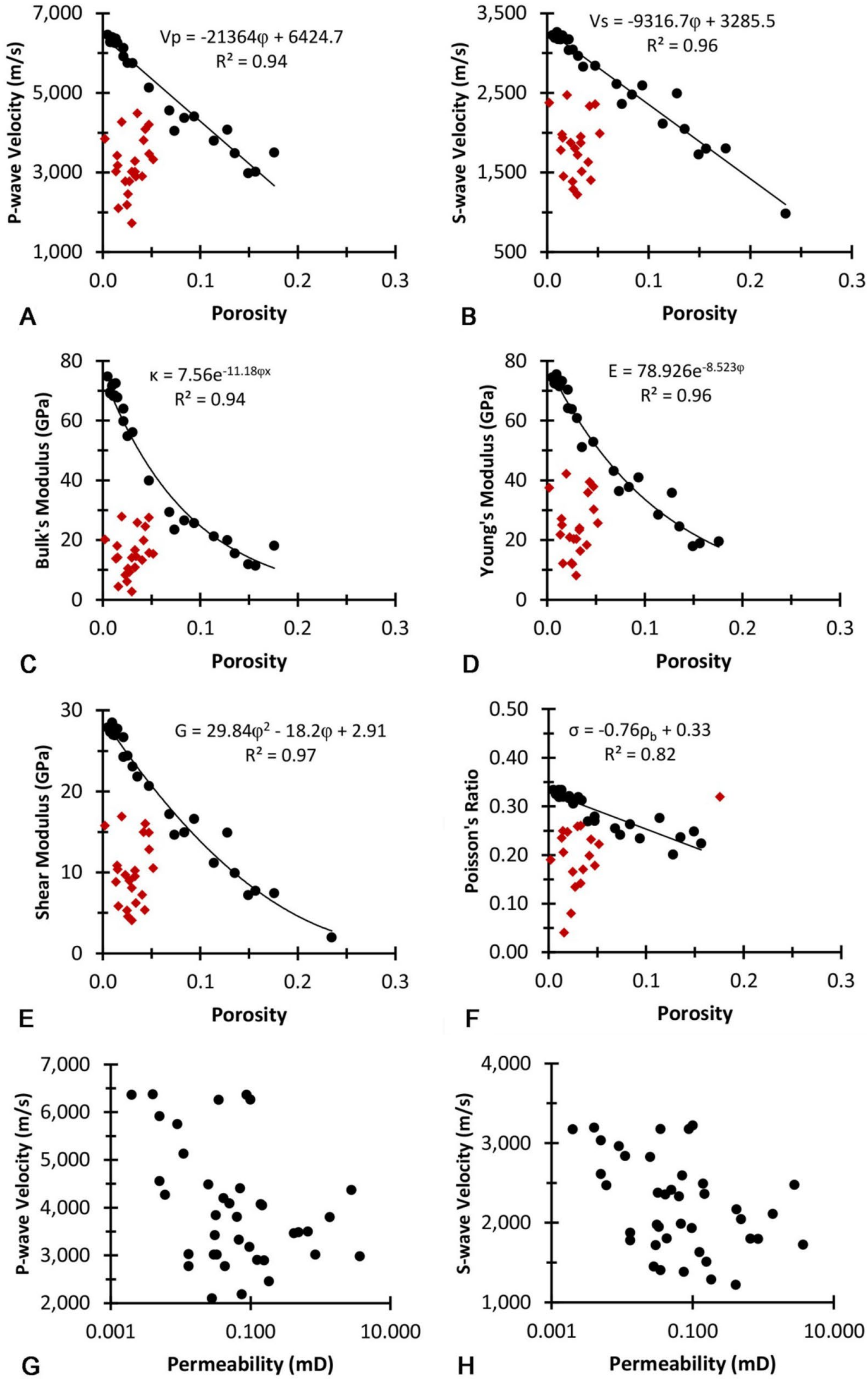

Fig. 10 Crossplots between the measured petrophysical parameters: φ vs. V_p (**a**), φ vs. V_s (**b**), φ vs. κ (**c**), φ vs. E (**d**), φ vs. G (**e**), φ vs. σ (**f**), k vs. V_p (**g**), and k vs. V_s (**h**)

(> 0.3) Poisson's ratios which may be explained by the size heterogeneity of the composing grains which differentially affect V_p and V_s, and in turn, the Poisson's ratio.

Yu et al. (2016) observed a different behavior of velocity ratios with the porosity of some natural and synthetic materials. Some materials such as iron compacts, fused glass beads, and Al_2O_3 aggregates exhibit a decrease in the V_p/V_s ratio with the increase of porosity. Others, including quartz sandstones and porcelain, show an increase in Poisson's ratio with increasing porosity. Tatham (1982) and Wang et al. (2009a) observed an increase in the V_p/V_s ratio with the increase of porosity.

Sedimentary rocks may possess intrinsic or induced anisotropy (Nur 1971), which may result from the specific alignment of the constituting grains or coring-induced microfracturing. To evaluate the effect of seismic anisotropy in the investigated rocks, we plot the velocity measured along the axis of the core versus that measured across its diameter (Fig. 12). Although minor differences in seismic velocities along the two orthogonal directions are revealed; the measured two velocities are equally distributed around the midline being almost equal to each other. The average values of V_p across the axis and diameter are 4303 and 4326 m/s, respectively, while those of V_s are 2349 and 2309 m/s. These values are very close to each other and indicate that observed reductions in the velocity of some rocks (Figs. 9c, d, 10a, b) are not related to seismic anisotropy but may result mainly from a specific pore type, texture, and geometry induced by the characteristic composition and diagenetic history of the rock. The global velocity–porosity relationships proposed by Erickson and Jarrard (1998) reveal that the velocity of low-porosity sediments depends primarily on porosity and lithology, whereas in high-porosity sediments, velocities depend mainly on the consolidation history, weakly on porosity, and they are virtually independent of lithology. Therefore, we think that the velocity of the samples deviating from the expected porosity–velocity and density–velocity trends are strongly affected by their particular pore nature, which characterizes a particular lithology.

Diagenesis and velocity evolution in carbonate rocks

The diagenetic potential of siliciclastic rocks is usually very low, where increasing burial pressure reduces the primary porosity and increases the seismic velocity (Japsen 1993). Unlike siliciclastics, carbonate rocks generally undergo significant diagenetic processes and are more susceptible to dissolution, which may finally transform lithified sediments into rocks of completely different physical properties (Anselmetti and Eberli 1993). These processes can alter the amount and geometry of the rock's pore system and, in turn, produce a characteristic pattern of velocity evolution in the rock. Therefore, carbonate rocks generally display larger scatter in their petrophysical relationships (Kassab et al. 2016). Moreover, the presence of fine components, the depositional environment, and the differences in pore throat sizes contribute also to the observed scatter.

Perhaps the first process which changes the initial velocity/porosity of sediments is early compaction, which comprises initial consolidation, dewatering, and grain rearrangement. During this phase, the sediments may have high microporosity (mud to packstones) or interparticle porosity (grainstones). Original porosity can be reduced by a factor of about 20% with velocity increased by the same percent. Other diagenetic processes such as cementation and dissolution, alterations brought by recrystallization and dolomitization, as well as the associated transformations in pore types and pore aspect ratio, will also affect the velocity/porosity of the rock in a certain manner which can be described by a specific velocity–porosity path starting at deposition and ending at the measurement stage after the last diagenetic process (Anselmetti and Eberli 1993). This evolutionary path is not always a straight line of decreasing porosity and increasing velocity. Rather, it may be represented by a curved, or even irregular, line or loop depending on the timing and the specific effects of different diagenetic events.

Although in some situations the rock's original fabric may be dramatically altered, no changes in porosity can follow. Under certain conditions, most diagenetic processes occur much faster than compaction and the carbonate sediments can be quickly dissolved, cemented, and recrystallized which may result in a less compacted, highly cemented, rocks of low porosity but variable velocity according to the compaction level and the degree of cementation (Anselmetti and Eberli 1993, 1999). Observed cementation in the studied rocks by iron oxides and calcite (also clay minerals in sandstones) has reduced the pore size and accordingly affected porosity, density, permeability, and the seismic velocity. As we have seen, the plots of velocity versus both bulk density and porosity in our study showed a group of samples possessing variable velocity ranging from low to moderate, at a high bulk density and low porosity. We think that the low porosity evolved from the cementation, whereas the low/moderate velocity resulted from the less compaction. Most of these samples are from the Kesrouane Formation and are dominated by either micritic limestones or grainstones.

Impact of clay minerals on the elastic properties

Sandstones are not always clean and often contain minerals other than quartz such as clays and feldspars which affect their elastic behavior significantly. The presence of clays causes, generally, a major reduction in the porosity of sandstones (e.g., Hakimi et al. 2012). Significant amounts of clay

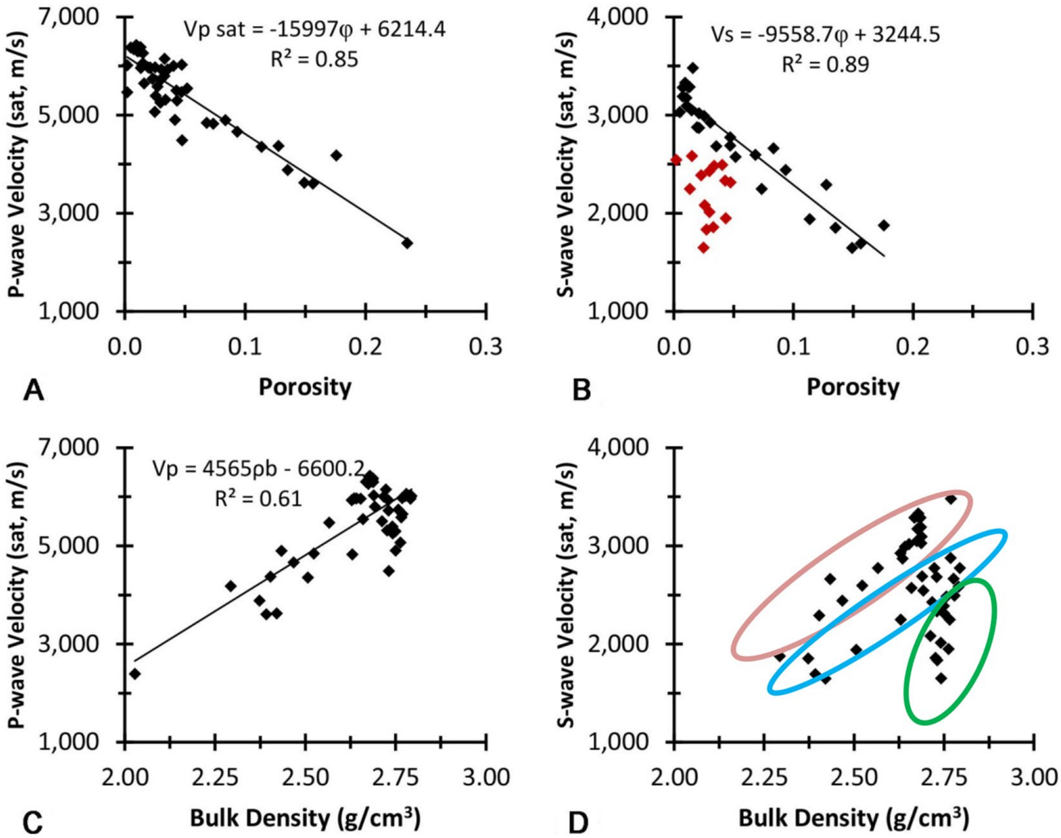

Fig. 11 The relationship between the acoustic velocities and both porosity (**a**, **b**) and bulk density (**c**, **d**) of the water-saturated samples

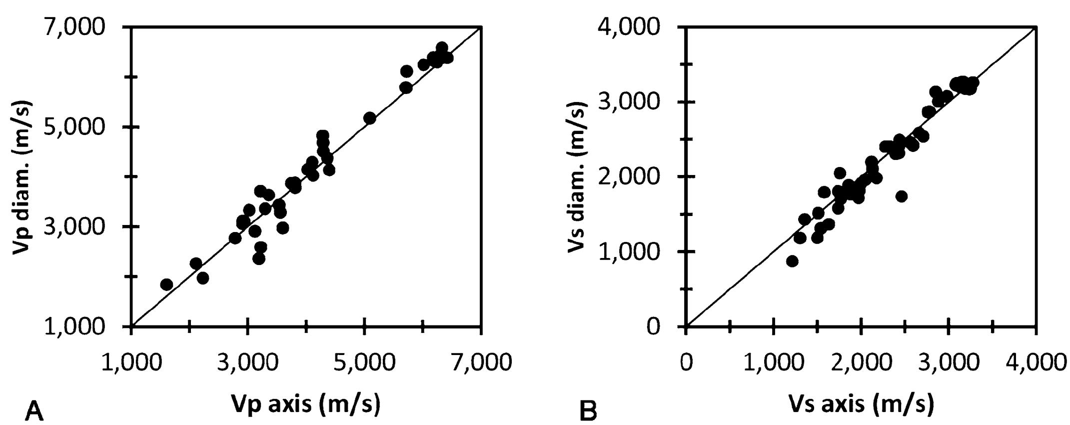

Fig. 12 **a** The relationship between V_p measured along the axis (V_p axis) and across-diameter (V_p diam); and **b** V_s along the axis (V_s axis) and across-diameter (V_s diam). See text for more details

in the rock will also lower the velocity relative to predictions from the time-average equation (Winkler and Murphy 1995).

The XRD analysis revealed that the mineralogy of samples K2, K4, K7, K8, K11, K16, K20, K26 and samples B2, B 7, and TC2 are distinct from that of samples TC1 and TC6 (Fig. 6). Samples of the first group are mainly carbonates (dolomitic grainstones or micritic limestones) while those of the second group are siliciclastics. Furthermore, samples K2 and K8, in the first group, are composed mainly of dolomite with minor amounts of mud and iron oxides. Samples K20 and B2, on the other hand, comprise a majority of calcite with minor proportions of dolomite. The siliciclastic group is composed mainly of quartz with minor amounts of feldspar and clay minerals. Calcite is also encountered between the quartz grains as a cement in the samples of this group (Fig. 6). These results imply that the observed deviations of velocity at low porosities cannot be induced by the clays which are not among the major constituting minerals of the studied rocks.

Porosity and the rock's elastic properties

Porosity has the major control on the seismic velocities and is usually linearly related to seismic velocities (Han et al. 1986). In practice, measured porosity-modulus data display generally a high degree of scatter (Knackstedt et al. 2005). The scatter could be induced by many factors such as variations in lithology (Marion et al. 1992), the clay content and distribution (Han 1986), and the characteristic pore types and pore geometry (Anselmetti and Eberli 1993, 1999). To address the lithology-induced scatter, for example, previous researchers grouped experimentally investigated rocks are into lithological types such as sandstones, shaly sandstones, sandy shales, shales, dolostones, and limestones (Nur et al. 1995; Wang 2000). Concerning the cement type, Dvorkin and Nur (1998) could predict the type of cement from the distribution of points on porosity–velocity plots. The clay–cement trajectory is characterized by reduced porosities and velocities relative to the quartz–cement trajectory.

Using the DEM (differential effective medium) theory, Neto et al. (2014) calculated spherical, interparticle, and microcrack pore geometries with aspect ratios of 1.0, 0.1, and 0.01 for the dry clean calcite limestone and presented it as lines in the velocity–porosity crossplots. The V_p–φ scattering reflects an increase in the rounded inclusions (tending towards the spherical line) or the microporosity inclusions (tending towards the microcrack line) by the fraction and aspect ratio balances of the geometric inclusions. Weger et al. (2009) compiled a large carbonate data set and found a relationship between the amount of macro- and mesopore inclusions which make the rocks stiffer with higher seismic velocities and the micropore inclusions which soften the rocks and reduce their seismic velocities.

Samples containing pores with low aspect ratios (cracks) are associated with lower velocities compared to samples with round pores or high aspect ratios. As a result, high-velocity contrasts are sometimes observed between rocks without large variations in their total porosity. Intercrystalline porosity develops at a later stage during diagenesis when newly crystallized minerals such as dolomite rhombohedra form a loose aggregate. It has a similar petrophysical behavior as interparticle porosity. The accumulation of unconnected grains without cement or matrix results in a low velocity because the rock has low elastic moduli due to the lack of a rigid framework. Most of these samples, therefore, show a negative departure from the average velocity–porosity correlation (Anselmetti and Eberli 1993).

Micro-pores (< 10 μm) are abundant in carbonate mud, either in a micritic grain or in the micritic matrix. High micro-porosity is thus expected in carbonates with high micritic content. Due to the lack of cementation that results in an unconnected grain fabric, micro-porosity has a similar effect on velocity as fine-grained, interparticle porosity and also shows a negative departure from the average velocity–porosity trend. As a consequence, velocity estimation for a given carbonate sample should not be performed using only the porosity values, but in combination with an assessment of the pore type. The observed complicated velocity–porosity pattern, which causes a similar impedance–porosity pattern (Fig. 13a), implies that an impedance contrast between two layers can occur even without a porosity change, due only to different pore types (Anselmetti and Eberli 1993, 1999). The impedance pattern may also change with saturation (Fig. 13b).

Previously, it has been observed that deriving porosity of carbonates using the time-average equation underestimates the true porosity. The difference between the estimated and the actual porosity is known as the secondary porosity, which is thought to be located mainly in rounded vugular pores with a minor effect on the measured velocity. Pore shape is a very important parameter affecting the porosity–velocity relationship in this case. If the pores are contained in thin flat cracks, a small amount of porosity will have a large effect on the measured velocities (Walsh 1965). On the other hand, if spheroidal pores are common in the rock, the same amount of porosity will have a minimal effect on velocity. Because carbonates are more soluble than sandstones, they tend always to have more complex pore structures which are not accounted for in conventional velocity models. Accordingly, various models have been proposed based on the pore aspect ratio (Kuster and Toksöz 1974; Cheng and Toksöz 1979; Berryman 1980) or the crack distribution parameters (O'Connell and Budiansky 1974).

Effect of pressure on velocities

Another factor which controls the velocity–porosity relationship is pressure. Coring- and exhumation-induced pressure release may generate microcracks which affect measured velocities. Pressure-dependent velocity variations of up to 50% may be induced by small, initial microcrack porosities of $^<$ 0.005 implying that the primary effect of this pressure change on velocity is through its impact on the rock's elastic moduli, not on porosity or density (Nur and Murphy 1981; Bourbié et al. 1987). Erickson and Jarrard (1998) concluded that microcracks affect the velocity–porosity relationship of any sediment that has undergone a large decrease in overburden stress, and that effect is not accurately predictable. The petrographic and SEM analyses showed no evidence of microcracking in the majority of the investigated samples.

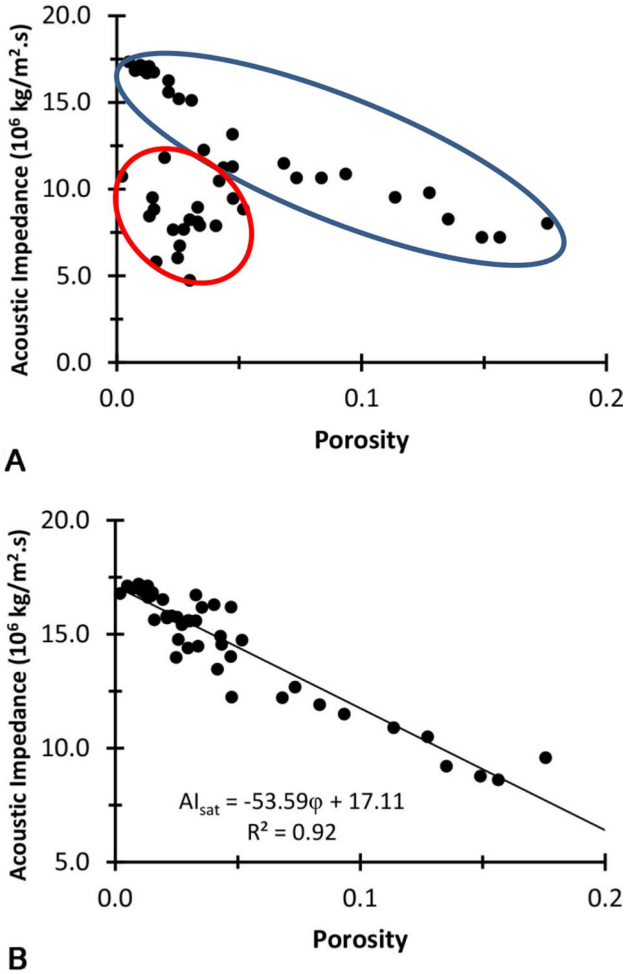

Fig. 13 A crossplot of porosity *vs.* acoustic impedance of the dry (**a**) and water-saturated (**b**) samples. The scatter in the velocity/porosity data of carbonate rocks, especially at dry conditions, may induce impedance contrasts and complicates the reflectivity pattern. The later may also change with saturation

However, different rates of fracturing have been detected in a few samples (Fig. 14). Samples K4 and TC2 are slightly fractured, whereas samples B2 and TA2 are, respectively, moderately and intensively fractured. Sample K4 has additionally a large amount of micropores, while sample B2 contains lesser amount. Lithologically, sample TA2 is calcareous sandstone, while the other three samples are carbonates. The petrophysical and elastic parameters of samples B2 and TA2 do not deviate from the routine porosity–velocity and density–velocity trends. On the other hand, sample K4 and TC2 are among the outliers. For this reason, outliers are not induced mainly by coring-induced microfracturing even though we do not preclude this possibility in other few samples. We think that the observed deviations from expected trends are induced mainly by specific pore types resulting from characteristic diagenetic processes in certain (but not all) carbonate samples.

Conclusions

We have conducted several investigations on forty-nine core samples collected from Mesozoic rocks exposed in central Lebanon to understand their lithofacies, mineralogy, their diagenetic history and their impacts on the petrophysical and elastic properties of the studied rocks.

The petrographic examination of representative samples revealed the existence of a variety of lithofacies ranging from grainstone, wackstone/packstone, micritic limestone/mudstone, to quartzarenite. The XRD analysis indicated that the dominant minerals are quartz, calcite, and dolomite. In addition, minor amounts of iron oxides, clay minerals, and feldspars are also encountered.

The studied rocks are characterized generally by low/moderate porosity, moderate/high bulk density, and very low permeability. Inverse and direct linear trends are obtained between velocity–porosity and velocity–density, respectively. However, some carbonate samples deviate significantly from these trends toward lower velocities at low porosity/high bulk density ranges. Because these rocks are carbonates, the clay content is excluded as a possible cause for the observed departures. Velocity measurements on three perpendicular directions across the cylindrical plugs revealed that seismic anisotropy is very low and, therefore, cannot explain the observed scatter. Although microfractures (whether primary or coring-induced) may be responsible for the reductions of seismic velocities at low porosities in few samples, we think that a characteristic pore geometry and pore types are thought to be the main causes of the observed differential decrease of seismic velocity at low porosities and high bulk densities. Previous studies found that different velocities in rocks with equal porosities are the result of different pore types. Rocks with framework-supported pores such as moldic or intraparticle porosity have higher velocity even at high-porosity fabrics, whereas rocks having interparticle, intercrystalline, or high microporosity have, at the same porosities, lower velocity.

It is clear that the propagation velocity of seismic waves in rocks is a complex process depending on various intrinsic parameters such as porosity, cracks, fractures, mineralogical composition, clay content, anisotropy, and other textural characteristics. Of these different parameters, porosity is the principal factor affecting the elastic properties of rocks. Our measurements indicate that seismic velocity varies widely in carbonate rocks where the maximum V_p value (6455 m/s) is almost four times higher than the minimum value at 1725 m/s. The V_s also varies widely in carbonate rocks from a minimum of 1221 m/s to a maximum at 3263 m/s. Such large variations in carbonates result additionally from many other factors including the depositional setting, composition, pore geometry, pore types, the higher diagenetic

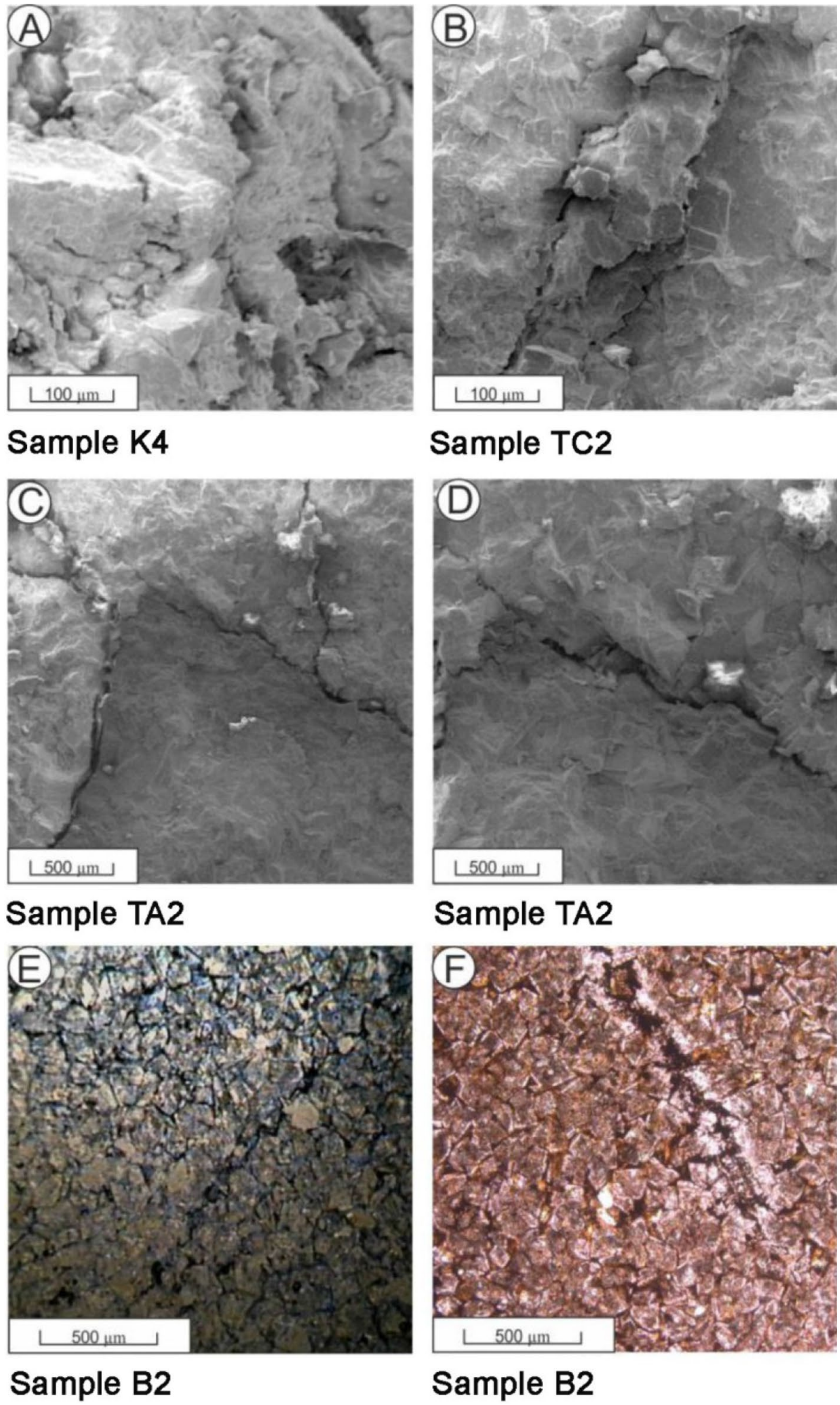

Fig. 14 SEM and thin section images displaying different degrees of fracturing: Samples K4 (**a**) and TC2 (**b**) display a slight fracturing; sample TA2 (**c**, **d**) is intensively fractured; while sample B2 (**e**, **f**) is moderately fractured

susceptibility, etc. Carbonates deposited in shallow water have generally a higher average velocity than carbonates deposited in deeper shelf, slope, or basin due to the higher diagenetic potential of the shallow-water carbonates. In contrast, mineralogy, burial depth, and age have minor effects on velocity in carbonates.

Our analysis also revealed that the physical properties of rocks are a combined result of the initial sediment type and their subsequent diagenetic alterations. The initial composition determines the diagenetic potential of the sediments and the timing of the different diagenetic events controls the porosity evolution and thus the velocity development. Finally, the numerous empirical relations which exist between various petrophysical parameters on local and regional scales vary from a region to another depending on the physical properties of the sediments, diagenetic processes, and deformation history.

Acknowledgements SEM images were taken in the Central Research Science Laboratory/American University of Beirut. The petrophysical and acoustic measurements have been conducted at the Department of Geosciences & Environment, University of Cergy-Pontoise, France. This research has been partially covered by a grant from the University Research Board (URB) of the American University of Beirut (Award# 103009; Project# 22759).

References

Abuseda H (2010) Petrophysical modeling of formation factor, porosity, and water saturation of Bahariya Formation western desert, Egypt. Ph.D. thesis, Ain Shams University, p 134

Adiyaman Ö, Chorowicz J (2002) Late Cenozoic tectonics and volcanism in the northwestern corner of the Arabian Plate: a consequence of the strike-slip Dead Sea fault zone and the lateral escape of Anatolia. J Volcanol Geotherm Res 117:327–345

Anselmetti FS, Eberli GP (1993) Controls on sonic velocity in carbonates. Pageoph 141(2/3/4):0033

Anselmetti FS, Eberli GP (1999) The velocity-deviation log: a tool to predict pore type and permeability trends in carbonate drill holes from sonic and porosity or density logs. Am Assoc Pet Geol Bull 83:450–466. https://doi.org/10.1306/00AA9BCE-1730-11D7-8645000102C1865D

Baccelle L, Bosellini A (1965) Diagrammi per la stimavisiva della composizione percentuale nelle rocce sedimentarie. Annali della Universiti di Ferrara, Sezione 1X. Sci Geol Paleontol 1:59–62

Beard DC, Weyl PK (1973) Influence of texture on porosity and permeability in unconsolidated sand. AAPG Bull 57:349–369

Berryman JG (1980) Long-wavelength propagation in composite elastic media II. Ellipsoidal inclusions. J Acoust Soc Am 68:1820

Berryman JG (1995) Mixture theories for rock properties. In: Ahrens TJ (ed) Rock physics and phase relations. Handbook of physical constants. AGU, Washington, DC, pp 205–228

Berryman JG, Blair SC (1987) Kozeny-Carman relations and image-processing methods for estimating Darcy's constant. J Appl Phys. https://doi.org/10.1063/1.339497

Beydoun ZR (1977) Petroleum prospects of Lebanon: re-evaluation. AAPG Bull 61(1):43–64

Beydoun ZR (1999) Evolution and development of the Levant (Dead Sea Rift) transform system: a historical–chronological review of a structural controversy. In: Mac Niocaill C, Ryan PD (eds) Continental tectonics. Geological Society London Special Publications 164:239–255

Blatt H (1992) Sedimentary petrology. W H Freeman & Company, New York, p 524

Boulanouar A, Rahmouni A, Samaouali M, Geraud Y, Harnafi M, Sebbani J (2013) Determination of thermal conductivity and porosity of building stone from ultrasonic velocity measurements. Geomaterials 3:138–144

Bourbié T, Coussy O, Zinszner B (1987) Acoustics of porous media. Educ Technol, Paris

Brandt H (1955) A study of the speed of sound in porous granular media. ASME J Appl Mech 22:479–486

Burchette TP (2012) Carbonate rocks and petroleum reservoirs: a geological perspective from the industry. Geol Soc Lond Spec Publ 370:17–37. https://doi.org/10.1144/SP370.14

Burger HR, Sheehan AF, Jones CH (2006) Introduction to applied geophysics: exploring the shallow subsurface. W W Norton & Company Ltd, New York

Castagna JP, Batzle ML, Eastwood RL (1985) Relationship between compressional wave and shear wave velocities in clastic silicate rocks. Geophysics 50:551–570

Cheng CH, Toksöz MN (1979) Inversion of seismic velocities for the pore aspect ratio spectrum of a rock. J Geophys Res 84:7533

Daëron M, Klinger Y, Tapponnier P, Elias A, Jacques E, Sursock A (2007) 12,000-year-long record of 10 to 13 paleoearthquakes on the Yammouneh fault, Levant fault system, Lebanon. Bull Seismol Soc Am 97:749–771

Develle A-L, Gasse F, Vidal L, Williamson D, Demory F, Van Campo E, Ghaleb B, Thouveny N (2011) A 250 ka sedimentary record from a small karstic lake in the Northern Levant (Yammoûneh, Lebanon: paleoclimatic implications. Palaeogeogr Palaeoclimatol Palaeoecol 305:10–27. https://doi.org/10.1016/j.palaeo.2011.02.008

Doummar J, Sauter M, Geyer T (2012) Simulation of flow processes in a large scale karst system with an integrated catchment model (Mike She)—identification of relevant parameters influencing spring discharge. J Hydrol 426–427:112–123

Dubertret L (1955) Carte geologique du Liban au 1/200000 avec notice explicative. Republique Libanaise, Ministere des Travaux Publiques, Beirut, p 74

Dubertret L (1975) Introduction à la carte geologique à 1/50000 du Liban

Dvorkin J, Nur A (1998) Time-average equation revisited. Geophysics 63(2):460–464

El Sayed AA, El Batanony M, Salah A (1998) Poisson's ration and reservoir fluid saturation: upper Cretaeceous, Egypt. In: MinChem, vol 98, 27–30 Sep, Siofok, pp 9–14

El Sayed NA, Abuseda H, Kassab MA (2015) Acoustic wave velocity behavior for some Jurassic carbonate samples, north Sinai, Egypt. J Afr Earth Sci 111:14–25. https://doi.org/10.1016/j.jafrearsci.2015.07.016

Elliot SE, Wiley BF (1975) Compressional velocities of partially saturated unconsolidated sands. Geophysics 40:949–954

Erickson SN, Jarrard RD (1998) Velocity-porosity relationships for water-saturated siliciclastic sediments. J Geophys Res 103(B12):30385–30406

Ersoy H, Yalçinalp B, Arslan M, Babacan AE, Çetiner G (2016) Geological and geomechanical properties of the carbonate rocks at the eastern Black Sea Region (NE Turkey). J Afr Earth Sci 123:223–233. https://doi.org/10.1016/j.jafrearsci.2016.07.026

Eysa EA, Ramadan FS, El Nady MM, Said NM (2016) Reservoir characterization using porosity–permeability relations and statistical analysis: a case study from North Western Desert, Egypt. Arab J Geosci 9:403. https://doi.org/10.1007/s12517-016-2430-x

Flügel E (1982) Microfacies analysis of limestone. Springer, Berlin, p 663

Gardner GHF, Gardner LW, Gregory AR (1974) Formation velocity and density—the diagnostic basics for stratigraphic traps. Geophysics 39:770–780

Ghalayini R, Daniel J-M, Homberg C, Nader FH, Comstock JE (2014) Impact of Cenozoic strike-slip tectonics on the evolution of the northern Levant Basin (offshore Lebanon). Tectonics. https://doi.org/10.1002/2014TC003574

Gomez F, Khawlie M, Tabet C, Darkal AN, Khair K, Barazangi M (2006) Late Cenozoic uplift along the northern Dead Sea transform in Lebanon and Syria. Earth Planet Sci Lett 241:913–931

Gregory AR (1976) Fluid saturation effects on dynamic elastic properties of sedimentary rocks. Geophysics 41:895–921

Gupta V, Sharma R (2012) Relationship between textural, petrophysical and mechanical properties of quartzites: a case study from northwestern Himalaya. Eng Geol 135–136:1–9. https://doi.org/10.1016/j.enggeo.2012.02.006

Hakimi MH, Shalaby MR, Abdullah WH (2012) Application of well log analysis to assess the petrophysical parameters of the lower Cretaceous Biyad Formation, east Shabowah oilfields, Masila Basin, Yemen. World Appl Sci J 16(9):1227–1238

Han DH (1986) Effects of porosity and clay content on acoustic properties of sandstones and unconsolidated sediments. PhD thesis, Stanford University

Han DH, Batzle M (2004) Gassmann's equation and fluid-saturation effects on seismic velocities. Geophysics 69:398–405

Han DH, Nur A, Morgan D (1986) Effect of porosity and clay content on wave velocities in sandstones. Geophysics 51:2093–2107

Hawie N, Gorini C, Deschamps R, Nader FH, Montadert L, Grajeon D, Baudin F (2013) Tectono-stratigraphic evolution of the northern Levant Basin (offshore Lebanon). Mar Pet Geol 48:392–410

Hawie N, Deschamps R, Nader FH, Gorini Ch, Müller C, Desmares D, Hoteit A, Granjeon D, Montadert L, Baudin F (2014) Sedimentological and stratigraphic evolution of northern Lebanon since the Late Cretaceous: implications for the Levant margin and basin. Arab J Geosci 7:1323–1349. https://doi.org/10.1007/s12517-013-0914-5

Hicks WG, Berry JE (1956) Application of continuous velocity logs to determination of fluid saturation of reservoir rocks. Geophysics 21:739–754

Hughes DS, Kelly JL (1952) Variation of elastic wave velocity with saturation in sandstone. Geophysics 17:739–752

Japsen P (1993) Influence of lithology and Neogene uplift on seismic velocities in Denmark: implications for depth conversion of maps. AAPG Bull 77:194–211

Kassab MA, Abuseda HH, El Sayed NA, LaLa AM, Elnaggar OM (2016) Petrographical and petrophysical integrated studies, Jurassic rock samples, North Sinai, Egypt. Arab J Geosci 9:9. https://doi.org/10.1007/s12517-015-2146-3

Khair K, Tsokas GN, Sawaf T (1997) Crustal structure of the northern Levant region: multiple source Werner deconvolution estimates for Bouguer gravity anomalies. Geophys J Int 128:605–616

Klinkenberg LJ (1941) The permeability of porous media to liquids and gases. Drilling and Productions Practices. American Petroleum Institute, Washington, pp 200–213

Knackstedt MA, Arns CH, Pinczewski WV (2005) Velocity–porosity relationships: predictive velocity model for cemented sands composed of multiple mineral phases. Geophys Prospect 53:349–372

Kumar M, Han D (2005) Pore shape effect on elastic properties of carbonate rocks. SEG Tech Program Expand Abstr. https://doi.org/10.1190/1.2147969

Kuster GT, Toksöz MN (1974) Velocity and attenuation of seismic waves in two-phase media: Part 1. Theoretical formulations. Geophysics 39:587

Longiaru S (1987) Visual comparators for estimating the degree of sorting from plane and thin sections. J Sedimentol Petrol 57:792–794

Lucia FJ (1995) Rock fabric/petrophysical classification of carbonate pore space for reservoir characterization. AAPG Bull 79(9):1275–1300

Marion D, Nur A, Yin H, Han D (1992) Compressional velocity and porosity in sand–clay mixtures. Geophysics 57:554–563

Mavko G, Mukerji T, Dvorkin J (1998) The rock physics handbook: tools for seismic analysis in porous media. Cambridge University Press, New York, pp 307–309

Mavko G, Mukerji T, Dvorkin J (2009) The rock physics handbook: tools for seismic analysis of porous media. Cambridge University Press, New York

Minear MJ (1982) Clay models and acoustic velocities. In: Presented at the 57th annual meeting, American Institute of Mining and Metallurgical Engineers, New Orleans

Nabawy BS, Barakat MKh (2017) Formation evaluation using conventional and special core analyses: Belayim Formation as a case study, Gulf of Suez, Egypt. Arab J Geosci 10:25. https://doi.org/10.1007/s12517-016-2796-9

Nabawy BS, David C (2016) X-Ray CT scanning imaging for the Nubia sandstone as a tool for characterizing its capillary properties. Geosci J 20(5):691–704. https://doi.org/10.1007/s12303-015-0073-7

Nabawy BS, Sediek KN, Nafee SA (2015) Pore fabric assignment using electrical conductivity of some Albian–Cenomanian sequences in north Eastern Desert, Egypt. Arab J Geosci 8:5601–5615. https://doi.org/10.1007/s12517-014-1631-4

Nader FH (2000) Petrographic and geochemical characterization of the Jurassic–Cretaceous carbonate sequence of the Nahr Ibrahim region, Lebanon. MSc thesis, American University of Beirut

Nader FH (2014) The geology of Lebanon. Scientific Press Ltd, Beijing

Nader FH, Swennen R (2004) The hydrocarbon potential of Lebanon: new insights from regional correlations and studies of Jurassic dolomitization. J Pet Geol 27:253–275

Nader FH, Swennen R, Keppens E (2008) Calcitization/dedolomitization of Jurassic dolostones (Lebanon): results from petrographic and sequential geochemical analyses. Sedimentology 55:1467–1485. https://doi.org/10.1111/j.1365-3091.2008.00953.x

Nakajima J, Matsuzawa T, Hasegawa A, Zhao D (2001) Three-dimensional structure of V_p, V_s, and V_p/V_s beneath northeastern Japan: implications for arc magmatism and fluids. J Geophys Res 106:21843–21857

Neto IAL, Misságia RM, Ceia MA, Archilha NL, Oliveira LC (2014) Carbonate pore system evaluation using the velocity–porosity–pressure relationship, digital image analysis, and differential effective medium theory. J Appl Geophys 110:23–33. https://doi.org/10.1016/j.jappgeo.2014.08.013

Nur A (1971) Effects of stress on velocity anisotropy in rocks with cracks. J Geophys Res 76:2022–2034

Nur A, Murphy W (1981) Wave velocities and attenuation in porous media with fluids. In: Paper presented at fourth international conference on continuum models of discrete systems, Stockholm

Nur A, Simmons G (1969) The effect of saturation on velocity in low porosity rocks. Earth Planet Sci Lett 7:183–193

Nur A, Mavko G, Dvorkin J, Gal D (1995) Critical porosity: the key to relating physical properties to porosity in rocks. In: 65th SEG meeting, Houston, expanded abstracts, 878

O'Connell RJ, Budiansky B (1974) Seismic velocities in dry and saturated cracked solids. J Geophys Res 79:5412

Ojha M, Sain K (2014) Velocity-porosity and velocity–density relationship for shallow sediments in the Kerala–Konkan Basin of Western Indian margin. J Geol Soc India 84:187–191

Pickett GR (1963) Acoustic character logs and their applications in formation evaluation. J Petrol Technol 15:650–667

Renouard G (1955) Oil prospects of Lebanon. AAPG Bull 39:2125–2169

Salah MK, Seno T (2008) Imaging of V_p, V_s, and Poisson's ratio anomalies beneath Southwest Japan: implications for volcanism and forearc mantle wedge serpentinization. J Asian Earth Sci 31:404–428

Salah MK, Zhao D (2003) 3-D seismic structure of Kii Peninsula in southwest Japan: evidence for slab dehydration in the forearc.

Tectonophysics 364:191–213. https://doi.org/10.1016/S0040-1951(03)00059-3
Salah MK, Sahin S, Topatan U (2014) Crustal velocity and Vp/Vs structures beneath central Anatolia from local seismic tomography. Arab J Geosci 7:4101–4118. https://doi.org/10.1007/s12517-013-1038-7
Saleh AA, Castagna JP (2004) Revisiting the Wyllie time average equation in the case of near-spherical pores. Geophysics 69:45–55. https://doi.org/10.1190/1.1649374
Schmoker JW, Krystinic KB, Halley RB (1985) Selected characteristics of limestone and dolomite reservoirs in the United States. AAPG Bull 69(5):733–741
Scholle PA, Ulmer-Scholle DS (2003) A color guide to the petrography of carbonate rocks: grains, textures, porosity, diagenesis. AAPG Memoir 77:875
Selley RC, Sonnenberg SA (2015) Elements of petroleum geology, 3rd edn. Academic Press/Elsevier, New York, p 509
Siegesmund S, Dürrast H (2014) Physical and mechanical properties of rocks. In: Siegesmund S, Snethlage R (eds) Stone and architecture. Springer, Berlin. https://doi.org/10.1007/978-3-642-45155-3_3
Sun YF, Berteussen K, Vega S, Eberli GP, Baechle GT, Weger RJ, Bracco Massaferro JL, Gartner GL, Wagner PD (2006) Effects of pore structure on 4D seismic signals in carbonate reservoirs. SEG Tech Program Expand Abstr. https://doi.org/10.1190/1.2370208
Sun P, Xu H, Dou Q, Adesokan H, Sun Y, Huang Q, Jiang N (2015) Investigation of pore-type heterogeneity and its inherent genetic mechanisms in deeply buried carbonate reservoirs based on some analytical methods of rock physics. J Nat Gas Sci Eng 27:385–398. https://doi.org/10.1016/j.jngse.2015.08.073
Swanson BJ (1981) A simple correlation between permeability and mercury capillary pressures. J Pet Technol 2488–2504
Tandon RSh, Gupta V (2013) The control of mineral constituents and textural characteristics on the petrophysical & mechanical (PM) properties of different rocks of the Himalaya. Eng Geol 153:125–143. https://doi.org/10.1016/j.enggeo.2012.11.005
Tatham RH (1982) V_p/V_s and lithology. Geophysics 47(3):336–344
Ündül Ö (2016) Assessment of mineralogical and petrographic factors affecting petro-physical properties, strength, and cracking processes of volcanic rocks. Eng Geol 210:10–22. https://doi.org/10.1016/j.enggeo.2016.06.001
Ündül Ö, Amann F, Aysal N, Plötze M (2015) Micro-textural effects on crack initiation and crack propagation of andesitic rocks. Eng Geol 193:267–275
Vernik L, Nur A (1992a) Petrophysical classification of siliciclastics for lithology and porosity prediction from seismic velocities. AAPG 79:1295–1309
Vernik L, Nur A (1992b) Ultrasonic velocity and anisotropy of hydrocarbon source rocks. Geophysics 57:727–735
Walley CD (1983) A revision of Lower Cretaceous stratigraphy of Lebanon. Geol Rundsch 377–388
Walley CD (1997) The lithostratigraphy of Lebanon: a review. Leban Sci Res Rep 10(1):81–108
Walley CD (1998) Some outstanding issues in the geology of Lebanon and their importance in the tectonic evolution of the Levantine region. Tectonophysics 298:37–62
Walsh JB (1965) The effect of cracks on the compressibility of rock. J Geophys Res 70:381
Wang Z (2000) Velocity–density relationships in sedimentary rocks. In: Wang Z, Nur A (eds) Seismic and acoustic velocities in reservoir rocks: vol. 3, Recent developments. Society of Exploration Geophysicists, Tulsa, pp 258–268
Wang J-H, Hung J-H, Dong J-J (2009a) Seismic velocities, density, porosity, and permeability measured at a deep hole penetrating the Chelungpu fault in central Taiwan. J Asian Earth Sci 36:135–145. https://doi.org/10.1016/j.jseaes.2009.01.010
Wang HY, Sun SZ, Li YW, Li XG (2009b) Velocity prediction models evaluation and permeability prediction for fractured and caved carbonate reservoir: from theory to case study. SEG Tech Program Expand Abstr. https://doi.org/10.1190/1.3255295
Weger RJ, Eberli GP, Baechle GT, Massaferro JL, Sun Y (2009) Quantification of pore structure and its effect on sonic velocity and permeability in carbonates. AAPG Bull 93(10):1297–1317. https://doi.org/10.1306/05270909001
Wilson JL (1975) Carbonate facies in geologic history. Springer, New York, p 471
Winkler KW, Murphy WF (1995) Acoustic velocity and attenuation in porous rocks. Rock physics and phase relations. A handbook of physical constants. AGU, Washington, pp 20–34
Wyllie MRJ, Gregory AR, Gardner LW (1958) An experimental investigation of factors affecting elastic wave velocities in porous media. Geophysics 23:450–493
Xu S, Payne MA (2009) Modeling elastic properties in carbonate rocks. Special section: rock physics. Lead Edge 28:66–74. https://doi.org/10.1190/1.3064148
Yu Ch, Ji Sh, Li Q (2016) Effects of porosity on seismic velocities, elastic moduli, and Poisson's ratios of solid materials and rocks. J Rock Mec Geotech Eng 8:35–49. https://doi.org/10.1016/j.jrmge.2015.07.004
Zhan X, Fullmer S, Lu C, Kaczmarek S, Harris C, Martinez A (2012) Study geophysical response of middle east carbonate reservoir using computational rock physics approach. SEG Tech Program Expand Abstr. https://doi.org/10.1190/segam2012-1137.1
Zhang Y, Bao Z, Zhao Y, Jiang L, Gong F (2017) Diagenesis and its controls on reservoir properties and hydrocarbon potential in tight sandstone: a case study from the Upper Triassic Chang 7 oil group of Yanchang Formation, Ordos Basin, China. Arab J Geosci 10:234. https://doi.org/10.1007/s12517-017-3023-z
Zhao D, Negishi H (1998) The 1995 Kobe earthquake: seismic image of the source zone and its implications for the rupture nucleation. J Geophys Res 103:9967–9986
Zhao D, Kanamori H, Negishi H (1996) Tomography of the source area of the 1995 Kobe earthquake: evidence for fluids at the hypocenter? Science 274:1891–1894